Earth and Space Science

RESEARCH ARTICLE
10.1029/2022EA002741

Special Section:
Advances in scaling and modeling of land-atmosphere interactions

Will Warming Climate Affect the Characteristics of Summer Monsoon Rainfall and Associated Extremes Over the Gangetic Plains in India?

Manas Pant[1,2], R. Bhatla[1,2], Soumik Ghosh[3], Sushant Das[4,5], and R. K. Mall[2]

[1]Department of Geophysics, Institute of Science, Banaras Hindu University, Varanasi, India, [2]DST-Mahamana Centre of Excellence in Climate Change Research, Institute of Environment and Sustainable Development, Banaras Hindu University, Varanasi, India, [3]Department of Earth and Planetary Sciences, Weizmann Institute of Science, Rehovot, Israel, [4]Earth System Physics Section, The Abdus Salam International Centre for Theoretical Physics, Trieste, Italy, [5]Now at Department of Meteorology (MISU), Stockholm University, Stockholm, Sweden

Key Points:

- The RegCM4 performs satisfactorily in simulating mean and extreme monsoonal rainfall characteristics over Gangetic Plains
- Projected decline in mean monsoon rainfall whereas a rise in extreme rainfall indices over the Gangetic plain under a warming climate
- Projected increase in extreme rainfall indices over upper Indo-Gangetic Plain and Himalayan foothills during future time slices under RCP8.5 scenario

Correspondence to:
R. Bhatla,
rbhatla@bhu.ac.in

Citation:
Pant, M., Bhatla, R., Ghosh, S., Das, S., & Mall, R. K. (2023). Will warming climate affect the characteristics of summer monsoon rainfall and associated extremes over the Gangetic Plains in India? *Earth and Space Science*, *10*, e2022EA002741. https://doi.org/10.1029/2022EA002741

Received 16 NOV 2022
Accepted 19 JAN 2023

Author Contributions:
Conceptualization: Manas Pant, R. Bhatla, Soumik Ghosh, Sushant Das
Data curation: Manas Pant, Sushant Das
Formal analysis: Manas Pant, Soumik Ghosh
Investigation: Soumik Ghosh, Sushant Das, R. K. Mall

Abstract The Indo-Gangetic Plain (IGP) bears great agricultural importance and contributes to a major share of national GDP of India. In present study, a location-specific comprehensive analysis of rainfall extremes over IGP, using second generation CORDEX-CORE simulations in the present and future scenarios (under high emission RCP8.5 scenario) have been performed. Here, the high-resolution CORDEX-CORE simulations with International Centre for Theoretical Physics's regional climate model (RegCM4.7) have been considered for the detailed rainfall characteristics assessment. Twelve thresholds-based climate indices have been analyzed to investigate the characteristics of rainfall extremes during three-time slices: 1986–2005 (historical), 2041–2060 (near future) and 2080–2099 (far future). The RegCM4 projections suggested a substantial decline in mean Indian Summer monsoon rainfall (ISMR) and wet days (rainfall ≥ 1 mm; 7%–14%) over IGP under high-emission RCP8.5 scenario. The contribution of 90th and 99th percentile days and total rainfall on wet days, seems to be get enhanced in future by 14%–35%, which implies the increase and intensification in rainfall extremes over IGP by the end of the 21st century. Further, the decline in ISMR and negligible changes in annual rainfall over IGP suggest the possible shift of monsoon regime during the later months of the year in warming climate. Thus, findings of present study may play a crucial role in predicting the ISMR and rainfall extremes over the IGP. Therefore, it can be useful for scientists and policymakers to plan and implement mitigation strategies.

Plain Language Summary In present study, an endeavor has been made to access the Indian Summer monsoon rainfall (ISMR) patterns and monsoon extremes over Gangetic plain which is fluvially fertile land and feeds around 40% Indian population. The International Centre for Theoretical Physics' regional climate model (RegCM4.7) robustly performs with various forcings in simulating mean precipitation and 12 different threshold-based climate indices over Indo-Gangetic Plain (IGP) during the historical period. However, the statistical analysis suggests RegCM4 with forcings EIN75 and MPI-ESM-MR followed by MIROC5 and Nor-ESM performs robustly in simulating the rainfall patterns over the IGP. Further, various forcing combinations have produced some rainfall indices with slight differences. Therefore, a ranking-based framework has been proposed in order to choose best forcing-combination for future projections. A closure encounter revealed that substantial decline in mean ISMR while negligible changes in annual rainfall have been projected which resembles to the fact of shift in monsoon regime toward the later months of the year under warming climate. As far as monsoon extreme are concerned, a rise in heavy rainfall days and their intensity have been projected. Also, maximum enhancement in projected heavy rainfall characteristics have been found to be near Himalayan foothills which is may be due the increased aerosol accumulation over IGP.

1. Introduction

The earth has been warmed by 1°C as compared with the pre-industrial era (Alley et al., 2003). According to a report of Intergovernmental panel on climate change (IPCC), the temperature will rise by 3–6°C till the 21st century at a rate of 0.2°C/decade under higher emission conditions (Pachauri et al., 2014; Solomon et al., 2007). The abrupt growth in urbanization, industrialization, deforestation, transportation, utilization of fossil fuel escalates the atmospheric load of greenhouse gases (GHGs), which is proved as a globally challenging phenomenon,

Methodology: Manas Pant, R. Bhatla, Sushant Das
Project Administration: R. Bhatla, R. K. Mall
Resources: R. Bhatla, R. K. Mall
Software: Manas Pant
Supervision: R. Bhatla, Soumik Ghosh, Sushant Das, R. K. Mall
Validation: Manas Pant
Visualization: Manas Pant
Writing – original draft: Manas Pant
Writing – review & editing: Manas Pant, Soumik Ghosh, Sushant Das

causing a lead role in climate change and global warming (Canadell et al., 2007; Tollefson, 2020). An increase in temperature manifests fluctuations and alterations to the atmospheric energy budget and affects the weather and climate variables, such as snow, precipitation and wind circulation (Gorman and Schneider, 2009; Roxy et al., 2017). Thus, an abrupt increase in the regional and local temperature will be a causative factor in the irregularity of the Indian Summer Monsoon (ISM) circulation, hence ISM rainfall is affected, which accounts for nearly 80% of the annual rainfall of the country (Gadgil & Gadgil, 2006; Turner & Annamalai, 2012).

Being an agriculture-based country, the ISM season (from the month of June to September; JJAS) plays a vital role in the livelihood and socio-economy of the rapidly increasing large Indian population (Rajeevan et al., 2010). Researchers have found evidences in support of enhancement in ISM irregularities which consequently leads to the amplification in frequency and intensity of extreme rainfall events (floods and drought) over the country during recent decades (Simpkins, 2017). The Clausius-Clapeyron equation suggests the enhancement in the rate of moisture content in the atmosphere due to global climate warming, which leads to the rise in the number and severity of rainfall extremes (Gorman & Schneider, 2009; Roxy et al., 2017; Tabari, 2020). Occurrences of hydroclimatic extremes such as extreme rainfall, flood and drought have adversely affected the socio-economic aspects of developing nations such as India during recent decades India has faced numerous devastating extreme rainfall events such as Mumbai (July 2005), Kedarnath (June 2013), Chennai flood (2015) and Kerala (in August 2018) which caused huge loss of lives and property due to landslides and floods (Boyaj et al., 2018; V. Mishra & Shah, 2018; Pant et al., 2022). Several studies have found the enhancement in frequency and intensity of extreme rainfall events while a gradual decrease in low to moderate-intensity rainfall events over India (Goswami et al., 2006; Guhathakurta et al., 2017; Pattanaik & Rajeevan, 2010). In a study Roxy et al., 2017 found three times enhancement in the frequency of extreme rainfall events accompanied by about a 20% decline in ISMR over the monsoon core region of India. The decline in ISMR can be a manifestation of alteration in several atmospheric and oceanic factors such as frequency of El Nino and La Nina southern oscillations (ENSOs), Indian Ocean warming, land use, convective available potential energy (CAPE), aerosol concentration etc (Das et al., 2020; Roxy et al., 2014, 2015; D. Singh et al., 2014). Several authors have found the role of aerosols in affecting the regularities of cloud systems and hence rainfall characteristics over a region (Fan et al., 2018; Tao et al., 2012). The atmospheric aerosols may alter the rainfall patterns in multiple ways such as by affecting large-scale circulations, atmospheric stability, cloud microphysics etc (Baker et al., 2015; Rosenfield et al., 2012). The atmospheric aerosols may drive the occurrence of heavy rainfall events over the Himalaya and its foothills during the ISM season (Choudhury et al., 2020).

The Coupled Model Intercomparison Project Phase 5 (CMIP5) experiment projections suggest wetter monsoon season and enhancement in extreme rainfall over South Asian regions (Kitoh & Endo, 2016; R. Maity et al., 2016; Sharmila et al., 2015). However, some other studies have proposed a decrease in seasonal rainfall and a shift in monsoon regimes in future (Ashfaq et al., 2009). These studies are based on the coarser resolution Global Climate Models (GCMs) and the changes in rainfall patterns are also affected by local factors such as topography which causes heterogeneity in model simulations. The use of finer-resolution climate models may enhance the reliability of modeling framework in order to present a better weather/climate pattern at regional scale (Kang et al., 2015; Vinnarasi & Dhanya, 2016). The concept of dynamical downscaling with regional climate model (RCM) was proposed to overcome the limitations associated with GCMs (Giorgi & Bates, 1989). After its development in the late 1980s at NCAR, the RegCM (first-ever RCM) has been popular in simulating climatic patterns across the globe (Giorgi et al., 2009, 2012). Various researchers have attempted to access the ISM patterns and associated variability by using RegCM over India and South Asia Coordinated Regional Climate Downscaling Experiment (SA-CORDEX: 22°S–50°N; 10°E−130°E) (Bhatla et al., 2016, 2018, 2019; Maharana & Dimri, 2016; Shahi, 2022; Verma et al., 2021). The reliability of RegCM simulations enhances when used in mixed parameterization mode (Giorgi et al., 2012; J. S. Pal et al., 2007). Therefore, several scientists considered the different combinations of cumulus parameterization schemes (CPSs) to reproduce the ISM circulation and pattern (Ghosh et al., 2019, 2022; S. Maity et al., 2017; A. K. Mishra et al., 2020; Sinha et al., 2019; Verma et al., 2022; Verma & Bhatla, 2021). A high-resolution regional model RegCM has been used for the simulation and projection of weather and climate extremes (Ngo-Duc et al., 2017; Pant et al., 2022; Rai et al., 2020). In a study with RegCM4.3, Rai et al. (2020) found an increase in heavy rainfall events over various homogeneous rainfall regions of India under warming scenarios. Another study by Shahi et al. (2021) found RegCM4 performing robustly in simulating rainfall extremes and enhancement in future under high emission RCP8.5 scenario over India and its monsoon core region (MCR). An attempt to simulate localized extreme rainfall events over

Mumbai with RegCM4 has been performed by Pant et al. (2022). Their findings show that the RegCM4 performs satisfactorily in simulating the extremely heavy rainfall event and associated dynamical and thermodynamical aspects. The above discussion suggests that the recent version of RegCM4 is able to unfold the climatic features at a regional scale. The investigation and estimation of ISMR patterns and associated extremes in past as well as in future under high emission scenarios (such as RCP8.5) will be of great importance over one of the most fluvial fertile lands of the world, that is, the Indo-Gangetic Plains (IGPs) in India. The IGP covers 13% geographic area (~6 lakhs km^2) of the country and is the source of food for around 40% Indian population (D. Pal et al., 2009). The agriculture activities in IGP are totally dependent on ISMR and monsoon variability may adversely affect the food supplies, health and economy and other aspects of the region and hence the country. Several researchers have attempted to access the ISM activity and its variations over IGP regions (Bhatla et al., 2019, 2020; Kothyari et al., 1997; N. Singh & Sontakke, 2002). Bhatla et al. (2015) studied the effect of ENSO events on ISMR which affects crop production over the Agro-Climatic-Zones of IGP region. Daloz et al. (2021) studied the impact of climate change on wheat production and found that the indirect impacts (decrease in irrigation availability) of climate change are more severe than the direct impacts (changes in temperature and rainfall) on the wheat yields in IGP. In a study, Yaduvanshi and Ranade (2017) found a decrease in the long term ISMR trend over eastern IGP regions while negligible variations in annual mean rainfall. Further, in another study Bhatla et al. (2019) found an increase in moderate to heavy rainfall events while a decrease in very heavy to extremely heavy rainfall events in the long-term (1901–2010) trend analysis. Using modeling approaches such as CORDEX-CORE and CMIP5 modeling framework, several authors have proposed the enhancement in mean and extreme temperatures over IGP in future under climate change scenarios (Chauhan et al., 2014; Sanjay et al., 2017; Wu et al., 2017). A projected increase of about 6°C (in comparison to the present day) by the end of the 2080s has been proposed. A multimodal ensemble approach suggested a 10% (20%) increase in precipitation by 2030s (2080s) under high emission scenarios (Chaturvedi et al., 2012). The assessment of climate indices recommended by the Expert Team on Climate Change Detection and Indices (ETCCDI) is of great importance to understanding the climate and associated variability over the region of interest (Zhang et al., 2011). Several researchers across the world have adopted the ETCCDI to analyze the rainfall patterns and associated frequency-based extremes as these indices are robust in detecting the trends in projected climate extremes (Ayugi et al., 2020; Herold et al., 2017; Tegegne et al., 2021). In a study Donat et al. (2013) evaluated the global patterns of climatic indices developed by the ETCCDI using newly updated observational data set (HadEX2) with better geographical and temporal coverage since the beginning of the twentieth century. Their study reported an increasing trend in severe rainfall but associated indices such as Rx5day and consecutive dry days (CDDs) have shown weak signals while the R10 mm (heavy rainfall event as per ETCCDI definition) shows a decrease over central-north India. Also, using threshold-based indices, Sillmann et al. (2013) found a rapid enhancement in extreme precipitation than the total wet day precipitation over different regions across the globe. Another study by Yaduvanshi et al. (2021) using CMIP5 models suggests a significant enhancement in extreme rainfall indices such as R95p, R99p, Rx1day and Rx5day (see Table 2) over the Western Ghats, central India and northeast Indian regions in future under RCP4.5&8.5 scenarios. Using daily rainfall data, Roy and Balling (2004) have found an increasing (decreasing) trend over southern peninsular regions (eastern Gangetic plains) in extreme rainfall frequencies (Rx1day, Rx5day, Rx30 day, 90th, 95th, and 97.5th percentiles) during 1910–2000. Panda et al. (2016) found a shift from wetter to drying conditions in twentieth-century climate indices over the central north Indian region. The rainfall extremes are heterogeneous over Indian river basins and the Ganga, north-eastern river basins have shown the highest rate of spatio-temporal variations during the recent decades (Chaubey et al., 2022). A localized study with ETCCDI indices over northeast Indian regions proposed a significant increase in CDDs while a decrease in wet day precipitation in recent times (Luwangleima & Shrivastava, 2019). However, the ISMR characteristics and their thresholds based comprehensive analysis over IGP is still unnoticed. Therefore, this study extensively focuses on the investigation of ISMR and associated extremes with threshold-based climate indices by using high-resolution CORDEX-CORE RegCM4.7 simulations during past and future time slices under high-emission RCP8.5 scenarios.

2. Model Description and Methodology

The latest CORDEX-CORE data downscaled with RCM have been considered to unfold and analyze the ISMR features and associated extremes over IGP. For that purpose, a state-of-the-art Regional Climate Model (RegCM4.7) which is developed and modified at Abdus Salam International Centre for Theoretical Physics

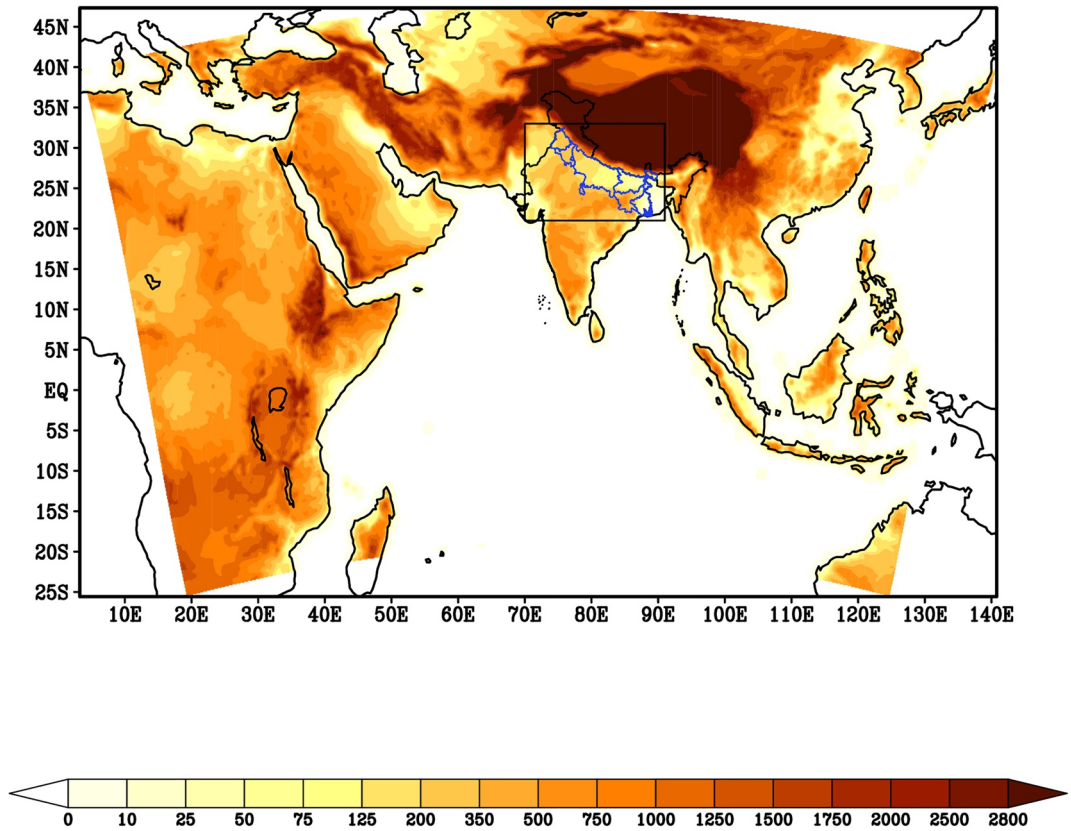

Figure 1. The model domain with topography (m) (SA-CORDEX domain; 22°S–50°N; 10°E−130°E) and study region that is, Indo-Gangetic Plain (within the box).

(ICTP), Italy has been considered. The RegCM4, a limited area sigma-coordinate model has been widely used to downscale over various CORDEX domains across the globe (Giorgi et al., 2012). The model domain and topography (South-Asia CORDEX domain; 22°S–50°N; 10°E−130°E) along with the study region (i.e., IGP) have been shown in Figure 1. The high-resolution CORDEX-CORE data has been generated by running the model at 25 Km horizontal resolution along with 23 vertical levels. The latest version RegCM4.7 has been employed over the SA-CORDEX domain in mixed cumulus parameterization mode as it helps to improve model simulations with a more precise representation of the sub-grid scale phenomenon (J. S. Pal et al., 2007). For that purpose, the convection schemes: MIT Emanuel over Land and Tiedtke over the ocean have been considered (Emanuel & Živković-Rothman, 1999; Tiedtke, 1989). A model configuration description has been shown in Table 1. The large-scale cloud formation has been represented by Subgrid Explicit Moisture Scheme (SUBEX; J. S. Pal et al., 2000) while boundary layer and radiation transfer have been chosen as proposed by Grenier and Bretherton (2001) and Kiehl et al. (1996) respectively. A better representation of land surface processes has been performed by considering the Community Land model version 4.5 (CLM4.5) as a land surface scheme (Oleson et al., 2013). The high-resolution dynamically downscaled rainfall data sets with different Initial and lateral boundary conditions (ICBCs) have been generated. The 6-hourly ICBCs derived from reanalysis data of the European center for medium range weather forecast (ECMWF) ERA-Interim (~0.75° × 0.75°) and three GCMs, namely; Max Planck Institute for Meteorology Earth System Model MR (MPI-ESM-MR; Watanabe & Opper, 2010) with resolution ~1.8° × 1.8°, Model for Interdisciplinary Research on Climate 5 (MIROC5; Stevens et al., 2013) with resolution ~ T85L40 for atmosphere & ~1° × 1° for the ocean and the Norwegian Earth System Model (NOR-ESM1-M; Bentsen et al., 2013) with resolution ~2° × 2° for atmosphere & ~1° × 1° for ocean). A study of Sharmila et al. (2015) has also found a better representation of ISM circulation features in MPI_ESM-MR, MIROC5, and NOR-ESM1-M GCMs simulations. In this study, the RegCM4.7 downscaled experiments have been denoted as RegCM_EIN75, RegCM_MPI, RegCM_MIROC, and RegCM_NOR hereafter. All the models run with the GCM forcings is from 1970 to 2005 for the historical period, thereafter following

Table 1
Detailed Description of RegCM4.7 Configuration

Description of regional climate model (RegCM4.7)	
Model dynamics	Hydrostatic
Horizontal and vertical resolution	25 Km with 23 vertical sigma levels
Initial and lateral boundary conditions (ICBC)	1. ECMWF ERA Interim reanalysis (EIN75) 2. MPI-ESM-MR 3. MIROC5 4. NorESM1-M
Radiation scheme	NCAR CCM3 (Community Climate Model 3; Kiehl et al., 1996)
Land surface model	Community land model version 4.5 (CLM4.5; Oleson et al., 2013)
Planetary boundary layer scheme (PBL)	Grenier and Bretherton (2001)
Large–scale precipitation scheme	Sub-grid explicit moisture scheme (SUBEX) (J. S. Pal et al., 2000)
Convective parametrization scheme	MIT Emanuel (Emanuel and Rothman, 1999) over land; Tiedtke (Tiedtke, 1989) over ocean

the RCP8.5 scenario forcing during 2006–2099. Here in our study, the 20-year time slabs for analysis that is, considering 1986–2005 (historical or reference period), 2041–2060 (near future; NF) and 2080–2099 (far future; FF) have been considered. The daily gridded data provided by India Meteorological Department (IMD) during the reference period have been considered for model validation (Pai et al., 2014). To evaluate model performance some robust techniques such as Taylor's diagram, Empirical Cumulative Orthogonal Function (ECDF) of daily rainfall mean have been considered.

Taylor Diagram: Taylor's diagram (Taylor, 2001) is extensively used for the validation of model simulated results. The similarity between observed and model-simulated fields is examined by evaluating the correlation coefficient (CC), root-mean-square error (RMSE) and standard deviation (SD). Mathematically, the formula of the Taylor diagram is:

$$E'^{(2)} = \sigma_f^{\,2} + \sigma_r^{\,2} + 2\sigma_f \sigma_r \rho \tag{1}$$

where ρ is the correlation coefficient (CC) between model and observation, E' is the centered root mean square (RMS) difference between model and observation, where $\sigma_f^{\,2}$ and $\sigma_r^{\,2}$ are the variances of the model simulation and observation, respectively.

Table 2
The Detailed Description of Twelve Threshold-Based Climate Indices

S.No.	Label used	Climate indices (definitions)	Units
1	R90p	Rainfall amount at 90th percentile of the duration	mm/day
2	R99p	Rainfall amount at 99th percentile of the duration	mm/day
3	WD	Number of wet days that is, days when rainfall; RR ≥ 1 mm	days
4	SDII	Simple/mean daily intensity of rainfall on wet days (i.e., the annual total precipitation divided by the number of wet days).	mm/day
5	R90p_days	Wet days w.r.t., 90th percentile of the duration	%
6	R99p_days	Extremely wet days w.r.t., 99th percentile of the duration	%
7	R90p_tot	Precipitation percent due to R90p_days	%
8	R99p_tot	Precipitation percent due to R99p_days	%
9	R10 mm	Heavy precipitation days (RR ≥ 10 mm)	days
10	R20 mm	Very heavy precipitation days (RR ≥ 20 mm)	days
11	Rx1day	Highest 1-day precipitation amount during the period	mm
12	Rx5day	Highest 5-day precipitation amount during the period	mm

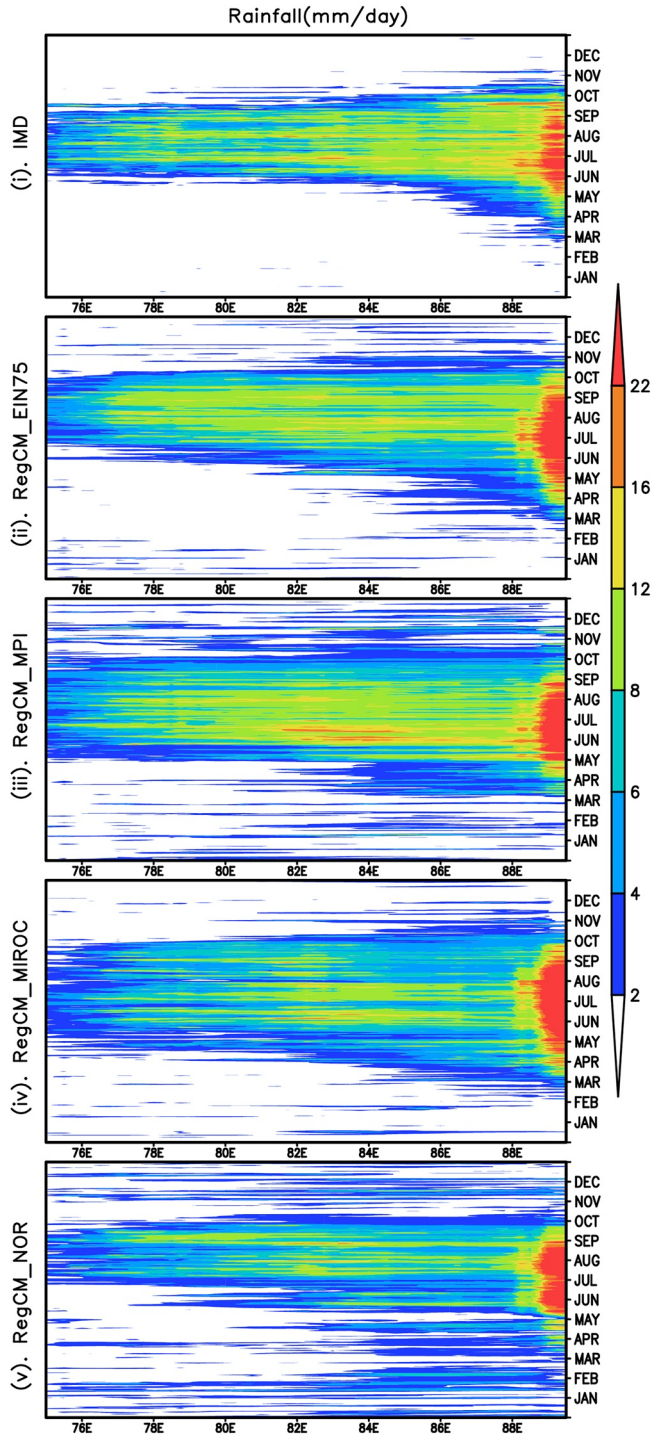

Figure 2. Spatial distribution of India Meteorological Department (observed) (i) and RegCM4 downscaled (ii–v) Zonally distributed meridional mean (over 22°N–32°N) rainfall pattern (mm/day) with four different Global Climate Model forcings over Indo-Gangetic Plain during the historical period 1986–2005.

ECDF: The ECDF is one the reliable approach which provides a significant estimate of uncertainty and confidence interval among data sets (Hoffman et al., 2017). Being an estimation of the cumulative distribution function the ECDF approach generates the points in the sample. It is a step function that increases by 1/n at the value of each ordered data point. The ECDF defined for observation $x = (x_1, x_2, \ldots x_n)$, F_n is the fraction of observations less or equal to t,

$$\mathrm{Fn}(t) = \frac{\text{number of elements in the sample} \leq t}{n} = \frac{1}{n}\sum_{i=1}^{n} 1_{[x_i \leq t]}, \quad (2)$$

Further, the relative changes (%) have been calculated for the estimation of variation in rainfall pattern and different climate indices in future time slices as compared with historical period.

$$\text{Relative Changes}\,(\%) = \frac{(\text{Future} - \text{Historical})}{\text{Historical}} \times 100 \quad (3)$$

Climate Indices: The use of threshold-based methods (by considering the distribution's tails) in identifying the extremes associated with various meteorological variables is gaining traction due to its greater significance regardless of local circumstances around the world (Zhang et al., 2011). In wake of the usefulness of threshold-based methods in analyzing and estimating the climatic variables, the 12 different climate indices have been considered in the present study. First, the spatio-temporal distribution of 12 climate indices namely, R90p, R99p, WD, SDII, R90p_days, R99p_days, R90p_tot, R99p_tot, R10 mm, R20 mm, Rx1day, and Rx5day has been considered during the historical period (the detailed description of these indices has been given in Table 2). Then, based on the performance of different RegCM4 members in simulating the mean threshold values of different climate indices over IGP, future projections have been considered accordingly.

3. Results and Analysis

3.1. The Spatial Distribution of Zonally Distributed Meridional (22°N–32°N) Annual Mean Rainfall Cycle Over IGP

The observed (IMD) and RegCM4 simulated annual cycle of the zonally distributed meridional mean (between 22°N and 32°N) over IGP during the historical period (1986–2005) has been shown in Figure 2. Observations reported enhancement in rainfall from the month of June (2–6 mm/day) which reaches its maximum (22 mm/day or more) during the months of July–September (JJAS) that is, during ISM season over India (Gadgil & Gadgil, 2006). Afterward, the rainfall started decreasing in the later months of the year. Some enhanced rainfall during September and October months can be observed. In their studies, Ashfaq et al. (2021) and Reshma et al. (2021) also found delayed onset and rainfall enhancement in the later months of the ISM season. The western or upper IGP regions (near 76°–80°E) receive 2–6 mm/day of rainfall which increases eastward, that is, toward central and lower IGP regions which suggest that lower IGP regions receive higher rainfall than rest of the IGP during ISM season. As far as modeling aspects are concerned, all the considered RegCM4 experiments have reproduced the rainfall pattern satisfactorily. It can be noticed that among all the considered RegCM4 experiments, the RegCM_EIN75 followed by RegCM_MPI and RegCM_MIROC shows rainfall patterns more realistically. Earlier versions of RegCM have reported some underestimation in simulating ISMR over MCR and IGP regions (Bhatla et al., 2019a; S. Singh et al., 2017). However, the recent RegCM version (v4.7) has shown remarkable improvements in the estimating the mean ISMR over India and its sub-regions

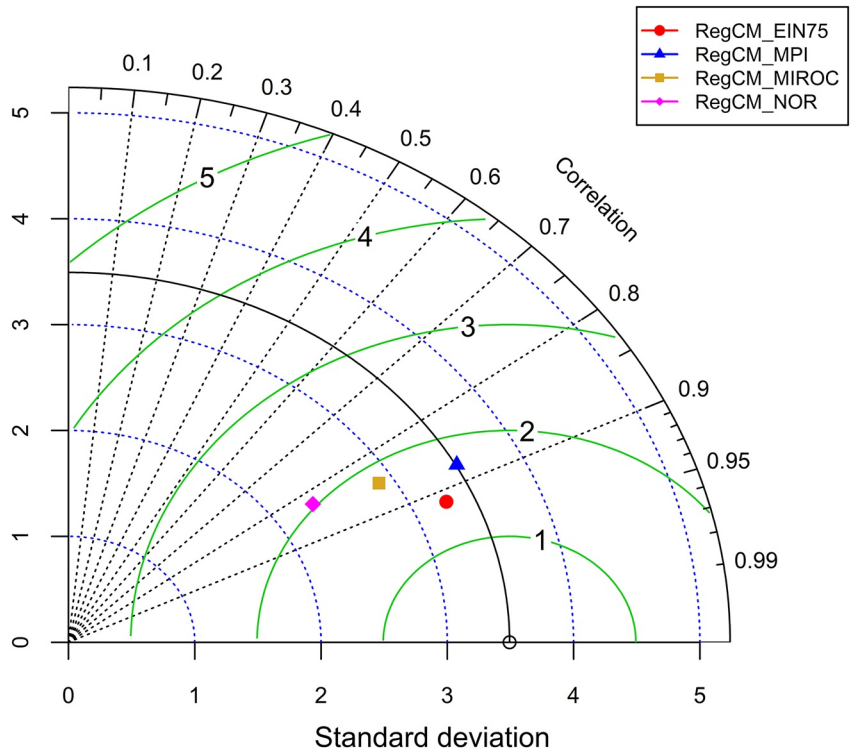

Figure 3. Taylor diagram for RegCM4 simulated daily mean rainfall with four different forcings by considering India Meteorological Department (observation) as reference during the historical period (1986–2005).

under CORDEX-CORE simulations (Verma et al., 2022). However, RegCM_MPI have shown some overestimation during pre and post monsoon months while RegCM_MIROC depicts excess rainfall during ISM season. Though the performance of RegCM_NOR is satisfactory during ISM season but it gets deteriorated during pre and post-monsoon months over IGP during the historical period.

3.2. Model Evaluation

The Taylor diagram has been used to evaluate the performance of RegCM4 in simulating rainfall patterns over IGP. The above figure (Figure 3) represents the Taylor diagram for RegCM4 simulated daily mean rainfall with different forcings by considering IMD (observation) as a reference over IGP during the historical period. It can be noticed that all the RegCM4 experiments show higher CC (>0.8) with observations. Among all the considered experiments, RegCM_EIN75 followed by RegCM_MPI and RegCM_MIROC shows the highest CC (0.92, 0.89, and 0.86 respectively) and least RMSE values while SD values nearer to the observations. However, the performance of RegCM_NOR is slightly less (CC $\sim$ 0.85 and higher RMSE) as compared to the other experimental configurations but it can be considered as satisfactory. The ECDF of observed and RegCM4 simulated daily ISMR data over IGP during the historical period have illustrated in Figure 4. It can be noticed that the observed rainfall distribution lies in the range of 0–15 mm/day or more with majority lying in the range of 2–10 mm/day during the period. The modeling aspects suggest that RegCM4 is able to reproduce the rainfall distribution satisfactorily as compared with the observations. However, the RegCM_MIROC followed by RegCM_EIN75 shows the best fit among all the considered RegCM4 experiments. Also, the fitting of curves simulated by RegCM_MPI and RegCM_NOR gets improved toward the higher rainfall amount days during the historical period.

3.3. Spatio-Temporal Distribution of Different Climate Indices

The observed and RegCM4 simulated distribution pattern of climate indices (R90p, R99p, WD, and SDII) have been illustrated in Figure 5. Observations reported 10–26 mm/day of R90p over IGP with upper tail of distribution lying over lower IGP regions where 18–26 mm/day of R90p has been observed (Figure 5a). Further, 14–22 mm/day and 10–18 mm/day of R90p have been reported over most of the central and upper IGP regions

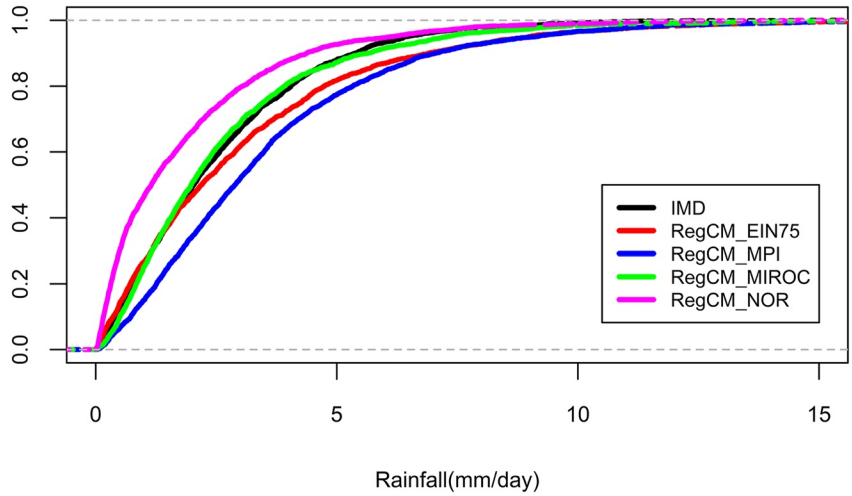

Figure 4. The empirical cumulative distribution function of observed and RegCM4 simulated daily Indian Summer monsoon rainfall (mm/day) during the historical period (1986–2005).

respectively. It can be noticed that RegCM_EIN75 reproduces R90p pattern reasonably well over IGP but with an underestimation (14–22 mm/day) over southern lower IGP regions (Figure 5b). The RegCM_MPI also depicts the similar distribution as that of RegCM_EIN75 over entire IGP except few northern central and lower IGP regions where it shows improved skill and reported 26 mm/day or more R90p during the historical period (Figure 5c). Similarly, the RegCM_MIROC have depicted 10–12 mm/day over upper IGP while 18–26 mm/day of R90p over north-central and lower IGP regions (Figure 5d). The performance of RegCM_NOR is similar to that of RegCM_MIROC but it has shown least skill among all the considered RegCM4 simulations (Figure 5e). Observations (Figures 5b–5i) depicted 55–70 mm/day or more of R99p over most of the IGP regions especially over lower and northern central IGP. Further, it can be noticed that lesser 25–35 mm/day of R99p have been reported over most of the upper IGP regions. Modeling aspects suggests that all the considered RegCM4 members have ability to reproduce the R99p patterns but with slight underestimation over entire IGP. The RegCM_EIN75 depicts 55–70 mm/day of R99p over north lower and central IGP while 15–35 mm/day over upper IGP region which agrees with the observations (Figure 5g). Another experiment RegCM_MPI shows similar performance as that of RegCM_EIN75 with some improvements over southern regions of lower and central IGP (45–55 mm/day) during the historical period (Figure 5h). Another experiment RegCM_MIROC shows some improvements (55–70 mm/day of R99p) over northern regions of lower and central IGP as compared in previously discussed RegCM4 experiments (Figure 5i). However, it underestimates the R99p over southern regions of lower and central IGP as compared with observations. The last member, RegCM_NOR shows satisfactory performance over extreme northern regions of lower and central IGP where it can reproduce 55–70 mm/day or more R99p (Figure 5j). However, it shows poorer performance over rest of the IGP regions as compared with observations during the historical period.

The distribution of observed and model simulated WD pattern has been depicted in Figures 5k–5o. Observations reported 80–90 of WD over lower IGP regions which decreases gradually toward central (~65) and upper IGP (50 or less) during the historical period (Figure 5k). As far as modeling aspects are concerned, the RegCM_EIN75 have shown satisfactory performance over lower IGP and reported 80 to 90 WD while it has shown huge overestimation (70–90 WD) over central IGP regions as compared to the observations (Figure 5l). Another model RegCM_MPI which has performed with highest efficiency so far among all the considered experiments, shows huge overestimation (70–90 or more) in reproducing WD over almost entire IGP region (Figure 5m). In the sequence, the RegCM_MIROC also depicts excess numbers (70–90) of WD over almost entire IGP (Figure 5n). However, performance of RegCM_MIROC is satisfactory over upper (50–55 or less) and lower (70–90) IGP regions in simulating WD during the historical period. The model RegCM_NOR shows 75–90 WD over lower IGP (closer to the observations) while it shows 50–80 WD over central IGP which is an overestimation as compared with observations (Figure 5o). The overestimation or large bias simulated in number of WD in RegCM_MPI and other RegCM experiments is also reported by the studies of Sonkoué et al. (2019) and Samuel

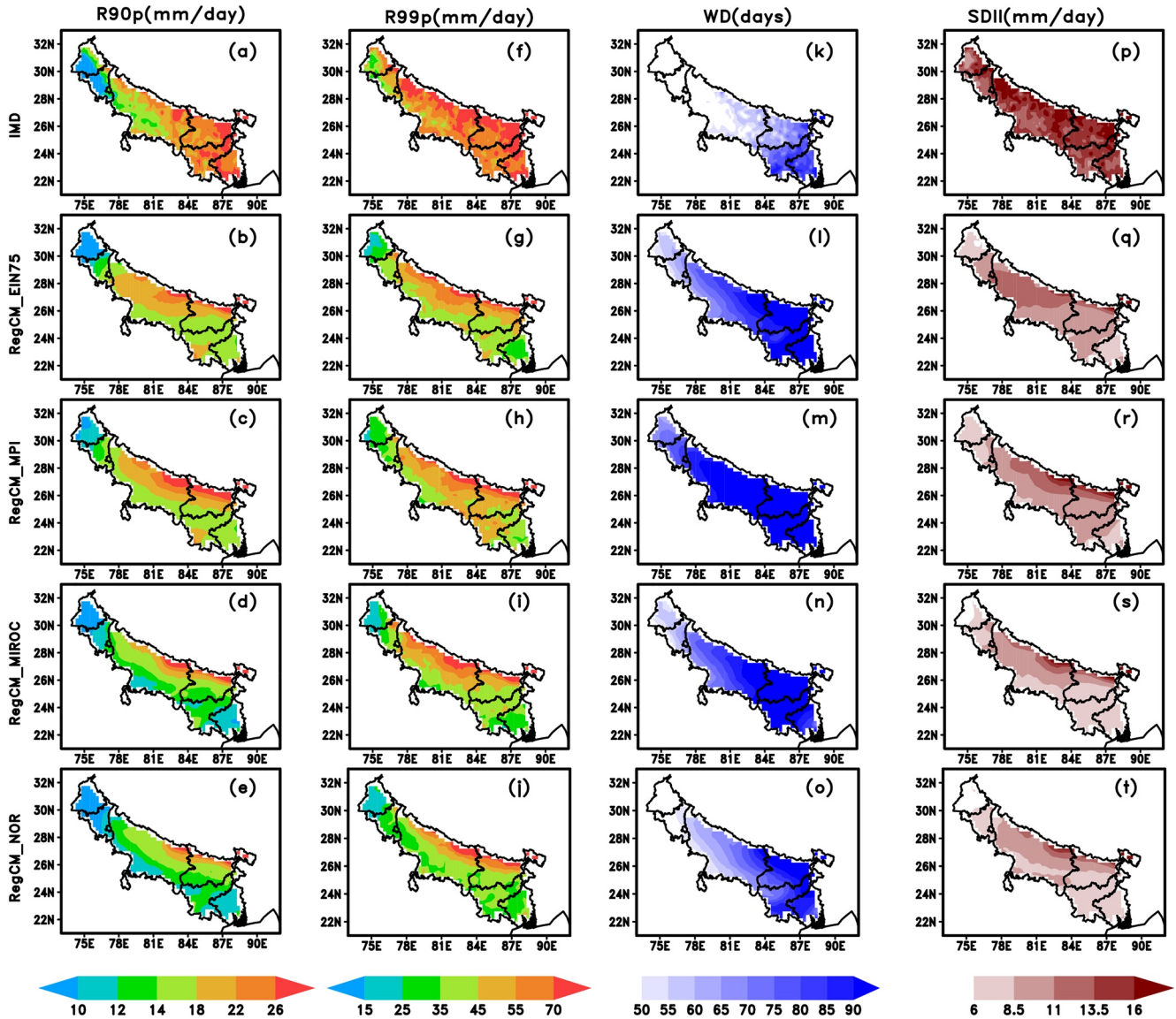

Figure 5. Spatial distribution of observed and RegCM4 simulated rainfall climate indices, namely (a–e). R90p (mm/day), (f–j). R99p (mm/day), (k–o). WD (days), (p–t). SDII (mm/day) over Indo-Gangetic Plain during the historical period (1986–2005).

et al. (2021) over African regions. Further, they proposed that these large biases and uncertainties in simulating WD can be attributed to the driving GCMs. In similar manner SDII of daily rainfall during ISM season has been illustrated in Figures 5p–5t. The observations reported SDII ranging from 11 to 16 mm/day over entire IGP region (Figure 5p). The upper tail, that is, 16 mm/day or more lies over lower and north-central region of IGP while the upper and south-central IGP regions have reported around 11 mm/day of SDII during the historical period. The RegCM_EIN75 experiment shows underestimated values of SDII over entire IGP except the extreme north-lower IGP (Figure 5q). Most of the upper and lower IGP regions depicted 6–11 mm/day SDII while 8.5–13.5 mm/day can be noticed over central IGP regions. Also, the RegCM_MPI has shown underestimation as similar to the RegCM_EIN75. However, RegCM_MPI shows a slight improvement (11–13.5 mm/day) over some north-central IGP regions (Figure 5r). Similarly, the remaining RegCM4 experiments that is, RegCM_MIROC and RegCM_NOR also depict the similar SDII pattern as that of early discussed members (Figures 5s and 5t). The underestimation of SDII over entire IGP in RegCM4 simulations has been reported by Verma et al. (2022). The SDII is defined as the mean rainfall intensity on WD over the considered reference period which implies that if any member among the considered experiments overestimates the numbers of WD than it will subsequently reduce

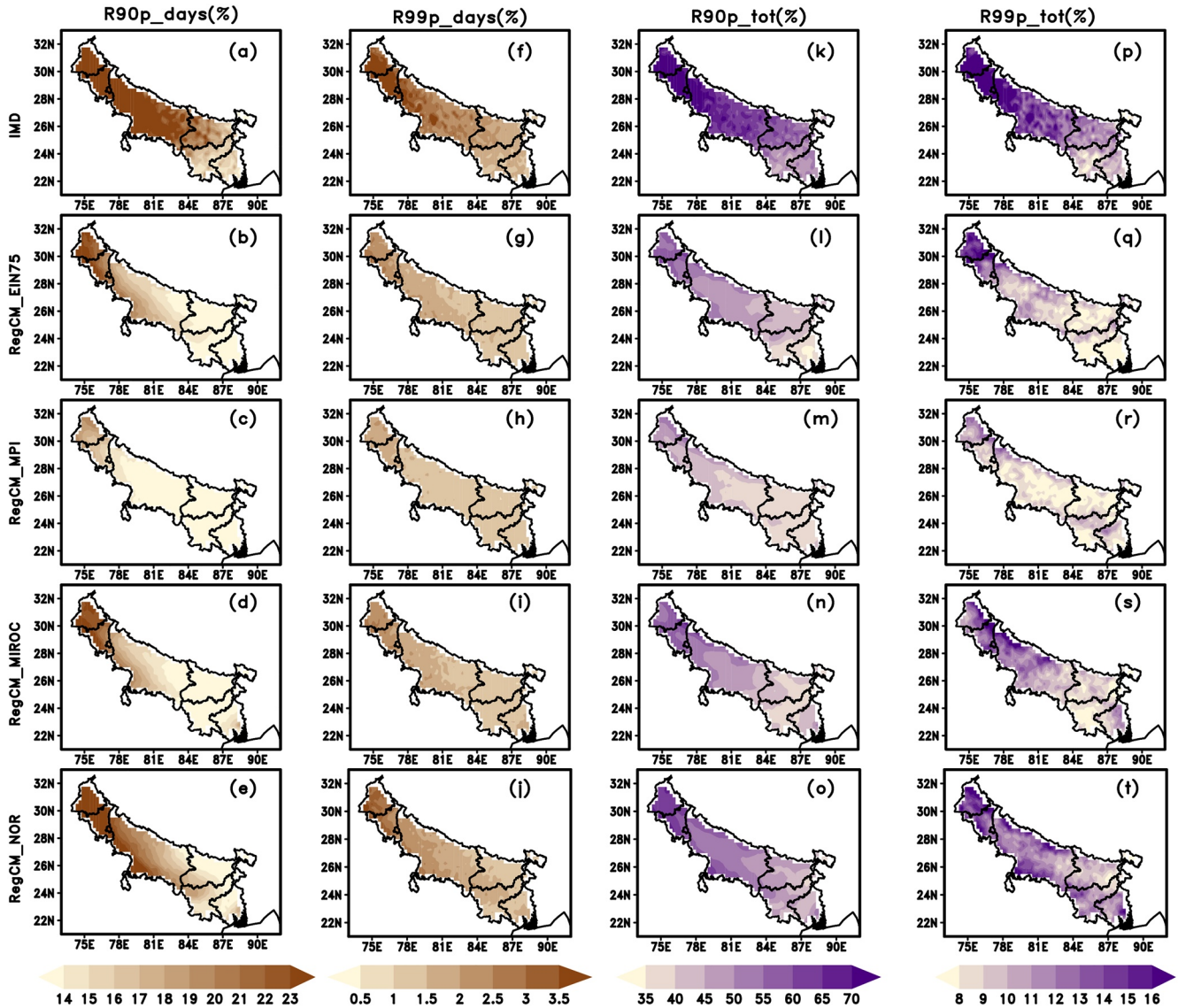

Figure 6. Same as Figure 5 but for rainfall climate indices namely (a–e). R90p_days (%) (f–j). R99p_days (%) (k–o). R90p_tot (%) (p–t). R99p_tot (%) over Indo-Gangetic Plain during the historical period (1986–2005).

the SDII over the concerned region (Table 1). It can be noticed that the observed as well as modeling aspects have shown the maximum of the heavy to heaviest rainfall thresholds (here R90p and R99p) and maximum SDII lies near the regions of foothills of Himalayas. It can be explained due the fact that the increased aerosols over IGP leads to the heavy precipitation events near the Himalayan foothills during ISM season (Choudhury et al., 2020).

The spatial distribution of observed and RegCM4 simulated R90p_days has been shown in Figures 6a–6e. Observations reported 21%–23% or more R90p_days over upper and central IGP regions whereas 15%–20% R90p_days over lower IGP regions during the historical period (Figure 6a). The RegCM_EIN75 reproduced 20%–22% over upper IGP which is in accordance with the observations but shows underestimated R90p_days over central (14%–18%) and lower (15% or less) IGP regions (Figure 6b). On the row, RegCM_MPI depicts underestimation (14%–18%) in R90_days over central and lower IGP regions. However, it reported nearly 20% R90p_days over upper IGP which is closer to the observations during the historical period (Figure 6c). Another member RegCM_MIROC shows 20%–22%, 14%–18%, and 15% or less over upper, central and lower IGP regions respectively (Figure 6d). However, it shows slight improvements over southern lower IGP region during the historical period. Surprisingly, the RegCM_NOR shows better performance over central IGP among all the considered experiments

as 18%–22% R90p_days which is closure to the observations (Figure 6e). Similarly, observations reported 3.5% or more R99p_days which gradually decreases toward central (1.5%–3%) and lower (1%–3%) IGP during the historical period (Figure 6f). It suggests that though upper IGP region receives lesser seasonal rainfall than lower IGP but the fraction of R90p and R99p rainfall among WD that is, R90p_days and R99p_days respectively is higher (depending on thresholds over concerned regions) over upper IGP than the central and lower IGP regions. The model RegCM_EIN75 performs satisfactorily and depicts 2%–2.5% R99p_days over some isolated upper IGP regions which decreases toward central (∼1.5%) and lower (1%–1.5%) IGP regions (Figure 6g). Another experiment RegCM_MPI follows the pattern but it shows huge underestimations throughout the IGP while RegCM_MIROC reproduces almost similar pattern as that of RegCM_EIN75 during the period (Figures 6h and 6i). As in the case of R90p_day, RegCM_NOR steals the attention and shows significant improvements by showing 3%, 2%–2.5% and 1%–1.5% of R99p_days over upper, central and lower IGP respectively (Figure 6j). Similarly, the spatial distribution of R90p_tot (the fraction of R90p rainfall amount in total seasonal rainfall) over IGP during the historical period has been depicted in Figures 6k–6o. The observations reported around 65%–70%, 50%–60% and 40%–60% of R90p_tot over upper, central and lower IGP regions (Figure 6k). The pattern of R90p_tot shows higher fractions over upper IGP which gradually decreases from central to lower IGP as similar to the R90p_days. The RegCM_EIN75 follows the observed pattern but shows underestimation and reported 50%–65% and 45%–55% over upper and central IGP while 35%–40% or less R90p_tot over southern lower IGP regions during the historical period (Figure 6l). Another experiment RegCM_MPI (Figure 6m) also reproduced the pattern with underestimated values of R90p_tot over upper (45%–55%), central (40%–50%) and lower (40% or less) IGP regions. The RegCM_MIROC shows similar pattern as that of RegCM_EIN75 over entire IGP except some southern lower IGP regions where it has reproduced 45%–50% of R90p_tot which is closer to the observations (Figure 6n). The last member in the row RegCM_NOR, has shown improved patterns as compared to the other considered experiments (Figure 6o). The RegCM_NOR have shown more realistic patterns with 55%–65%, 45%–55%, and 35%–55% of R90p_tot over upper, central and lower IGP regions respectively. Similarly, the spatial distribution of R99p_tot over IGP during the historical period has been discussed in Figures 6p–6t. Observations reported 14%–16% or more R99p_tot over upper IGP while 10%–13% and 8%–11% of R99p_tot over central and lower IGP regions during the historical period (Figure 6p). The RegCM_EIN75 satisfactorily reproduces the R99p_tot pattern over upper (14%–16%) and lower IGP (9% or less) but with slight underestimations (Figure 6q). Another member RegCM_MPI also follows the observed pattern but shows underestimations along entire IGP in simulating R99p_tot similar to previously discussed indices where the fraction among wet days has been considered. As far as RegCM_MIROC is concerned, its performance is very close to as that of RegCM_EIN75 (Figure 6s). However, it shows some improvements by showing 12%–14% of R99p_tot over central IGP regions as compared with previously discussed experiments. The last member in the row that is, RegCM_NOR shows remarkable improvements over entire IGP as it has shown for R90p_tot (Figure 6t). RegCM_NOR has reproduced 14%–15% or more, 10%–14% and 8%–13% of R99p_tot over upper, central and lower IGP regions respectively which is in close agreement with the observations.

Figures 7a–7e illustrates spatial distribution of R10 mm that is, the heavy rainfall days over IGP during the historical period. It can be noticed that R10 mm days ranging from 27 to 30, 18–27, and 15–18 or more over lower, central and upper IGP respectively have been observed (Figure 7a). The upper tail of the distribution lies over most of the lower IGP regions which gradually decreases as moving toward central and upper IGP regions. All of the RegCM4 members follow the observed pattern but with some uncertainties (Figures 7b–7e). The RegCM_EIN75 performs satisfactorily over upper and lower IGP regions except few eastern regions of lower IGP where it shows an underestimation (21–27 days) during the historical period (Figure 7b). Another member RegCM_MPI shows similar performance as that of RegCM_EIN75 over upper and lower IGP (Figure 7c). However, it shows huge overestimation over central and some north-lower IGP regions during the historical period. Similarly, the experiment RegCM_MIROC also performs satisfactorily over upper IGP but its performance gets deteriorated over lower and central IGP regions. The RegCM_NOR underestimates R10 mm days over south-lower IGP regions by a huge amount as compared with the observations (Figure 7e). Surprisingly, it shows improved pattern over some isolated central IGP regions. Similarly, Figures 7f–7j represents the spatial distribution of R20 mm days over IGP during the historical period. Observations depicted 14–17, 8–14, or more days over lower and central IGP respectively while 2–11 days over upper IGP regions during the period (Figure 7f). The RegCM_EIN75 performs satisfactorily over upper (2–11 days) and central (8–14 days) IGP but its performance gets deteriorated over lower IGP where it shows a huge underestimation (5–11 days) of R20 mm days (Figure 7g). Another member RegCM_MPI performs satisfactorily as compared to the other

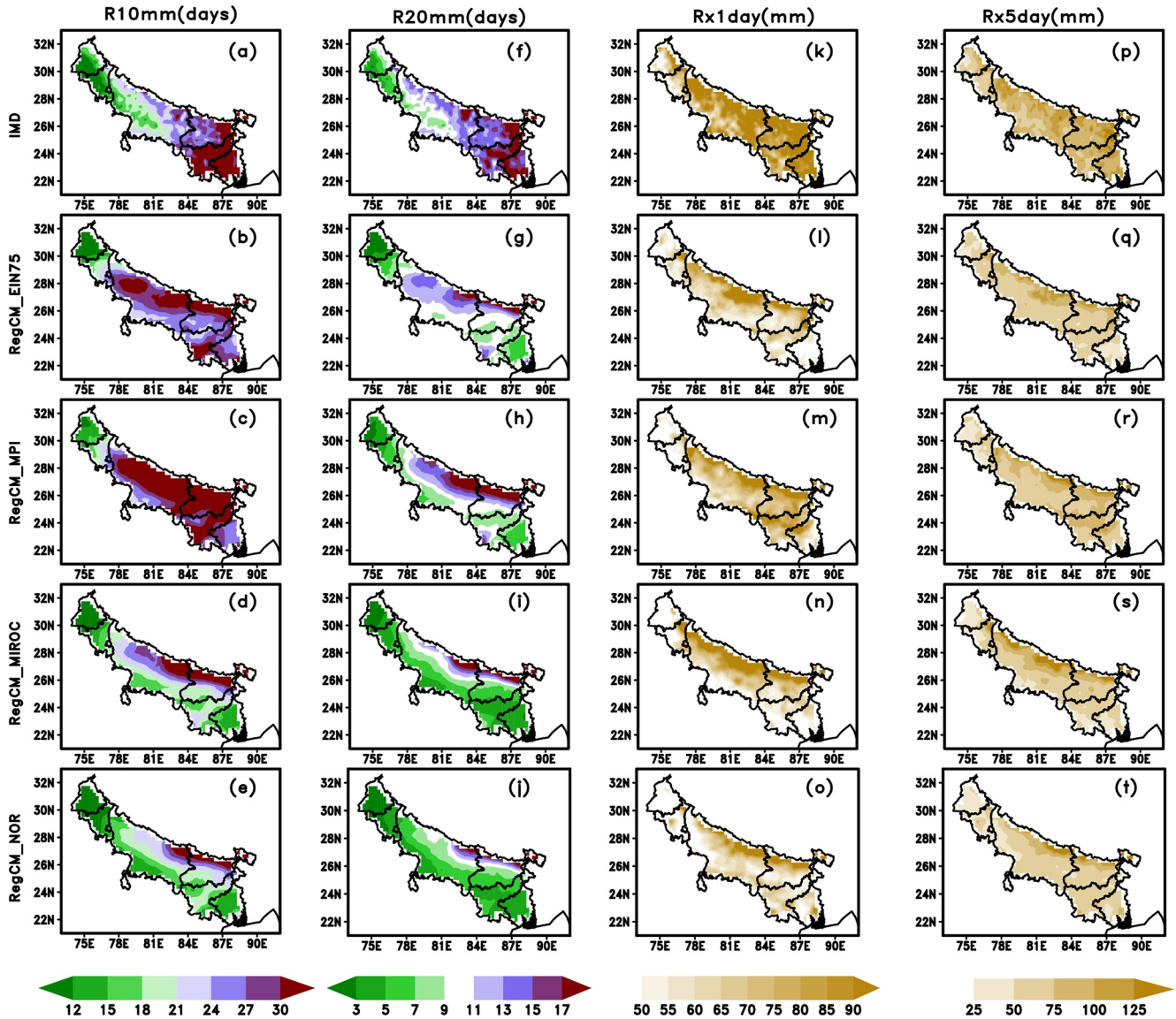

Figure 7. Same as Figure 5 but for rainfall climate indices namely (a–e). R10 mm (days) (f–j). R20 mm (days) (k–o). Rx1day (mm) (p–t). Rx5day (mm) over Indo-Gangetic Plain during the historical period (1986–2005).

members and has reproduced 8–14 and 2–8 of R20 mm days over central and upper IGP which is in accordance with the observations (Figure 7h). Similarly, other members in the row that is, RegCM_MIROC and RegCM_NOR illustrates similar results and their performance is slightly poor over lower and central IGP regions where they have shown 5–14 R20 mm days (Figures 7i and 7j). Though, performance of RegCM_MIROC is somehow satisfactory over upper and northern regions of central and lower IGP. The overall analysis suggests that all the RegCM4 experiments are able to simulate the pattern of R10 mm and R20 mm days over IGP and RegCM_MPI followed by RegCM_EIN75 have performed robustly as compared to the other members. Figures 7k–7o illustrates distribution of 1 day maximum rainfall that is, Rx1day over IGP regions during the historical period. Observations have reported 70–90 mm or more Rx1day over most of the lower and central IGP regions. However, upper IGP and southern regions of central IGP have shown 55–70 mm of Rx1day during the period (Figure 7k). As far as modeling aspects are concerned, the RegCM_EIN75 performs satisfactorily over upper (50–65 mm) and central (75–90 mm) IGP but it shows huge underestimation over lower and south-central IGP in simulating Rx1day (Figure 7l). Another member RegCM_MPI performs satisfactorily over most of the IGP regions and has reproduced more realistic patterns than RegCM_EIN75 (Figure 7m). Also, RegCM_MPI shows improved

Table 3
Ranking of RegCM4 Experiments Performance Based on Relative Departure in Mean Thresholds of Different Climate Indices as Compared With Observations During the Historical Period

S.No.	Climate indices	RegCM4 experiments	Relative departure in mean thresholds (%)	Rank
1	R90p	RegCM_EIN75	−9.52	2
		RegCM_MPI	**−9.41**	**1**
		RegCM_MIROC	−23.81	3
		RegCM_NOR	−33.33	4
2	R99p	RegCM_EIN75	−23.88	2
		RegCM_MPI	**−22.39**	**1**
		RegCM_MIROC	−25.37	3
		RegCM_NOR	−34.33	4
3	WD	RegCM_EIN75	49.12	3
		RegCM_MPI	66.67	4
		RegCM_MIROC	47.36	2
		RegCM_NOR	**26.316**	**1**
4	SDII	RegCM_EIN75	−29.73	2
		RegCM_MPI	**−29.53**	**1**
		RegCM_MIROC	−36.8	3
		RegCM_NOR	−40	4
5	R90p_days	RegCM_EIN75	−40	3
		RegCM_MPI	−48	4
		RegCM_MIROC	−40	2
		RegCM_NOR	**−24**	**1**
6	R99p_days	RegCM_EIN75	−25	3
		RegCM_MPI	−35	4
		RegCM_MIROC	−20	2
		RegCM_NOR	**−5**	**1**
7	R90p_tot	RegCM_EIN75	−22.95	3
		RegCM_MPI	−32.79	4
		RegCM_MIROC	−22.95	2
		RegCM_NOR	**−14.75**	**1**
8	R99p_tot	RegCM_EIN75	−23.08	3
		RegCM_MPI	−30.77	4
		RegCM_MIROC	−15.38	2
		RegCM_NOR	**−7.69**	**1**
9	R10 mm	**RegCM_EIN75**	**0.912**	**1**
		RegCM_MPI	23.01	3
		RegCM_MIROC	−12.7	2
		RegCM_NOR	−30	4
10	R20 mm	RegCM_EIN75	−46.59	2
		RegCM_MPI	**−45.11**	**1**
		RegCM_MIROC	−52.89	3
		RegCM_NOR	−70.37	4

simulations over south-lower IGP regions with 65–90 mm of Rx1day during the historical period. The RegCM_MIROC also depicts similar pattern as that of RegCM_EIN75 with some improvements over central IGP whereas underestimations over southern IGP. The last member in the row that is, RegCM_NOR shows improved patterns over some isolated southern lower IGP but it underestimates the Rx1day over almost entire IGP as compared with the observations (Figure 7o). Similarly, the distribution of Rx5day that is, maximum 5-day rainfall over IGP region during the historical period have been illustrated in (Figures 7p–7t). Observations reported 100–125 mm of Rx5day over northern lower and central IGP region while rest of lower and central IGP have shown 75–100 mm during the period (Figure 7p). Further, 25–75 mm or more Rx5day can be noticed over the upper IGP region. The RegCM_EIN75 performs satisfactorily over upper (25–75 mm) and northern regions of central IGP (75–125 mm) in simulating Rx5day (Figure 7q). However, it shows lesser (25–75 mm) Rx5day over rest of the IGP regions as compared with observations. Another member in the row, RegCM_MPI depicts more realistic pattern of Rx5day over entire IGP as compared to the other members (Figure 7r). In another experiment, RegCM_MIROC reproduces similar pattern as that of previously discussed experiments. However, it shows slight overestimation (∼100 mm) over northern regions of lower and central IGP (Figure 7s). Similarly, the member RegCM_NOR (Figure 7t) also reproduces the pattern of Rx5day but with least accuracy as compared to the other considered RegCM4 experiments during the historical period.

3.4. Model Ranking Classification Based on Threshold Estimation

The earlier discussion suggested that all the RegCM4 experiments have capability to reproduce the spatio-temporal patterns of different climate indices but it is difficult a little bit to choose single experiment or member for the projections of different climate indices. Therefore, to reduce uncertainties in future projections the percentage departure from area averaged mean thresholds of different climate indices (simulated in different RegCM4 experiments) have been listed in Table 3. For each of the climate indices the ranking (1–4) has been assigned to each RegCM4 member based on its performance in simulating the different climate indices over IGP. It can be seen that RegCM_MPI followed by RegCM_EIN75 shows least departure (as compared to the observations) among all the considered experiments and have been marked as Rank 1 and 2, respectively, while RegCM_MIROC and RegCM_NOR stands at Rank 3 and 4 respectively in simulating the R90p, R99p, SDII, R20 mm distributions over IGP. Similarly, the order of performance ranking has been found as RegCM_NOR (Rank 1), RegCM_MIROC (Rank 2), RegCM_EIN75 (Rank 3) and RegCM_MPI (Rank 4) in reproducing the patterns of WD, R90pdays, R99pdays, R90ptot and R99ptot climate indices during the historical period. In simulating the pattern of R10 mm, the member RegCM_EIN75 followed by RegCM_MIROC shows the least departure from observed thresholds and stands at Rank 1 and 2, respectively. The performance of different RegCM4 experiments in simulating indices namely, Rx1day and Rx5day has been found to be Rank 1–4 as RegCM_MPI, RegCM_MIROC, RegCM_EIN75 and RegCM_NOR respectively. Therefore, based on their performance, the RegCM_MPI projections of climate indices R90p, R99p, SDII, R20 mm, Rx1day and Rx5day while RegCM_NOR projections of WD, R90p_days, R99p_days, R90p_tot, R99p_tot will be considered.

Table 3
Continued

S.No.	Climate indices	RegCM4 experiments	Relative departure in mean thresholds (%)	Rank
11	Rx1day	RegCM_EIN75	−17.72	3
		RegCM_MPI	**−13.75**	**1**
		RegCM_MIROC	−15.75	2
		RegCM_NOR	−24.51	4
12	Rx5day	RegCM_EIN75	−17.72	3
		RegCM_MPI	**−13.68**	**1**
		RegCM_MIROC	−15.75	2
		RegCM_NOR	−24.51	4

Note: The bold values indicate the best performing member in simulating the concerned climate indices.

3.5. Projected Changes in Rainfall Patterns and Various Climate Indices Under High Emission RCP8.5 Scenario

3.5.1. Temporal Variation in Future Projected Annual and Seasonal (JJAS) Rainfall Distribution

The temporal distribution of annual and ISMR (JJAS) mean rainfall over IGP during three different time slices considered in the present study have been shown in Figures 8a and 8b. Observations (IMD) reported a variation of about 2–4 mm/day in mean annual rainfall over IGP during the historical period (Figure 8a). All the RegCM4 experiments follow the observed pattern with overestimated amount of 2–5 mm/day throughout the period. In future projections of annual mean rainfall, it can be seen that in each RegCM4 experiment, on average the fluctuations remain similar to that during the historical period. However, a slight enhancement during NF and a very slight decline in mean rainfall can be seen in FF projections. Similarly, the temporal variation in observed and RegCM4 simulated seasonal JJAS rainfall has been illustrated in Figure 8b. The observed pattern shows that the rainfall during JJAS lies between 6 and 9.5 mm/day during the historical period. All

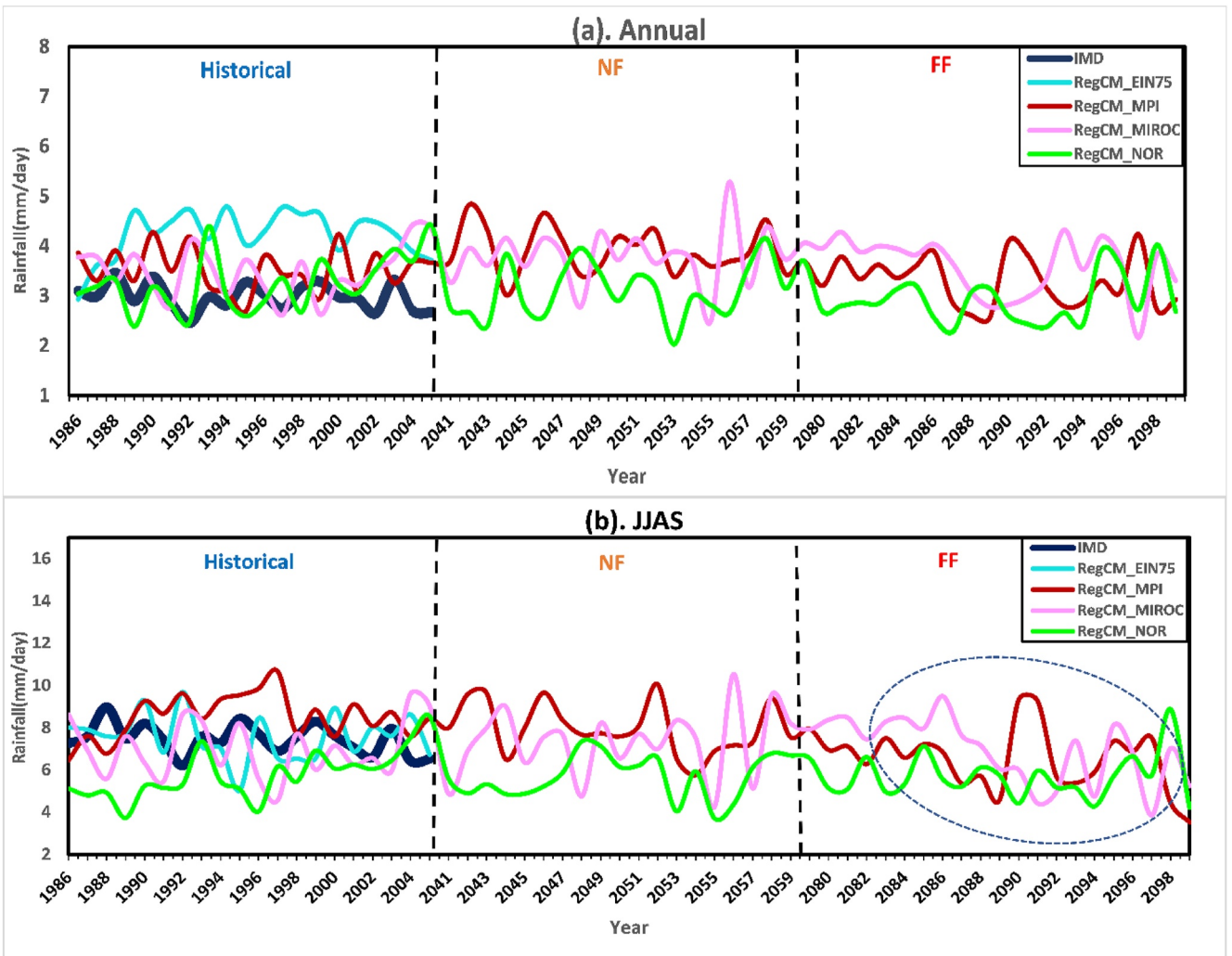

Figure 8. Temporal variation of observed and RegCM4 simulated/projected mean rainfall (a). Annual and (b). Seasonal (JJAS) over Indo-Gangetic Plain during the three different time slices: historical (1986–2005), near future (NF; 2041–2060) and far future (FF; 2080–2099).

the considered RegCM4 members have satisfactorily simulated the JJAS rainfall pattern over IGP but with some overestimation/underestimation ranging from 4 to 11 mm/day. The members RegCM_EIN75 and RegCM_MPI have reproduced the rainfall pattern reasonably well during the historical period. The future projections have shown very slightly declining JJAS rainfall patterns (within range the 4–10 mm/day) however, with in-between fluctuations during NF. The FF projections of RegCM4 suggest a gradual decline ranging from 2.5 to 8.5 mm/day or less in JJAS rainfall over IGP. The decreasing patterns are more prominent during the period afterward 2084 (encircled). The overall comparative assessment suggests a very slight change in annual mean rainfall but a huge decline in mean ISMR rainfall (especially during FF) over IGP. Also, results indicate an increase in rainfall activities over IGP during earlier or later months than JJAS of the year. Some studies have shown similar evidence in support of a decline in ISMR due to the weakening of monsoon circulation with onset delays and an increase in rainfall during post-ISM months in future under high emission scenario (Ashfaq et al., 2021; Shahi et al., 2021).

3.5.2. The Projected Changes in Various Climate Indices in NF and FF

The relative changes (%) in RegCM4 projected patterns of various climate indices during NF and FF (under high emission RCP8.5 scenario) as compared with the historical period has been illustrated in Figures 9 and 10. For that purpose, the previous discussion (Table 3) has been considered for the rectification among various RegCM4 experiments based on their rank as per the performance in simulating mean thresholds of various climate indices during the historical period. Therefore, only the model which has secured rank 1, has been considered for the future projection of respective climate indices. The distribution of RegCM4 projected R90p shows 7%–14% of decline over almost the entire IGP during NF (Figure 9a). However, a slight increase over some lower IGP regions can be noticed. The decreasing tendency of R90p seems to be continued as FF projections of RegCM4 suggest a very huge decline over most of the IGP regions ranging from 21% to 35% or more while a slight decline over fewer lower IGP regions as compared with the historical period (Figure 9b). Also, the projected differences during FF as compared to the NF depict huge decline (21%–35%) over upper IGP and northern regions of central and lower IGP (Figure 9c). Further, moderate to high decreases over southern regions of central and lower IGP have been projected. The projected distribution of R99p shows the opposite scenario as that of R90p and suggests huge enhancement over most of the upper, north-central and north-lower IGP (Figure 9d). Though, a slight decrease over some southern regions of central IGP during NF has been projected. As far as FF projections are concerned, a slight decline (7%–14% or more) over most of the IGP regions except a few upper, northern IGP and some of southern lower IGP regions where enhancement (21%–35%) in R99p can be noticed (Figure 9e). Further, the comparative changes in FF than NF suggests moderate to high decrease over entire IGP except few lower regions where a rising pattern of R99p has been projected (Figure 9f). The projected relative changes in R90p and R99p during NF and FF suggest the rapid enhancement in heaviest rainfall activities (R99p) while the decline in heavy rainfall (R90p) activities over IGP. However, an increase in R99p is much more prominent during NF than FF. Similarly, the distribution of R90p_days illustrates a projected increase over central IGP and south-upper IGP ranging from 7% to 21% whereas a slight decline (7%–14%) over lower and some upper IGP regions during NF (Figure 9g). Surprisingly, contrary to the R90p pattern the FF projections of R90p_days show a moderate to high increase (7%–28% or more) in R90p over the almost entire IGP (Figure 9h). Also, the changes during FF as compared with NF depicted a rise (7%–14%) in R90p_days over most of the central and lower IGP while a moderate decline of nearly 7% over the upper IGP region (Figure 9i). The distribution of relative changes in R99p_days (as compared with historical period) also illustrates the similar projected pattern as that of R90p_days over entire IGP region during NF (Figure 9j). However, the rise (21%–35%) in R99p_days over southern upper and central IGP and the decline (14%–28%) over north-western regions of upper IGP have been projected. The FF projections also suggest a similar R99p_days pattern as that of R90p_days over the entire IGP with amplified increase/decrease over the concerned region and sub-regions (Figure 9k). Further, it can be noticed that the distribution of R90p_days and R99p_days is very non-uniform and scattered over the entire IGP. The difference during FF as compared to NF also suggests enhancement (7%–28%) over most of the central and lower IGP while moderate to high decline (7%–21%) over the upper IGP region (Figure 9l). The projected increase in R90p_days and R99p_days over most of the IGP region resembles the studies of Kumar et al. (2011) and Rai et al. (2020) where rising trends and projections of very wet days have been found in different model simulations over India.

The distribution of rainfall contribution from heavy and extremely heavy rainfall days that is, R90p_tot and R99p_tot respectively have been shown in Figures 9m–9r. The pattern of R90p_tot suggests moderate to higher enhancement ranging from 7% to 28% over most of the IGP (specially over central IGP) during NF as compared to the historical period (Figure 9m). However, some extreme north and south regions of upper and lower IGP respectively, shows slight decrease ∼7% during the period. Similarly, the R90p_tot distribution shows higher

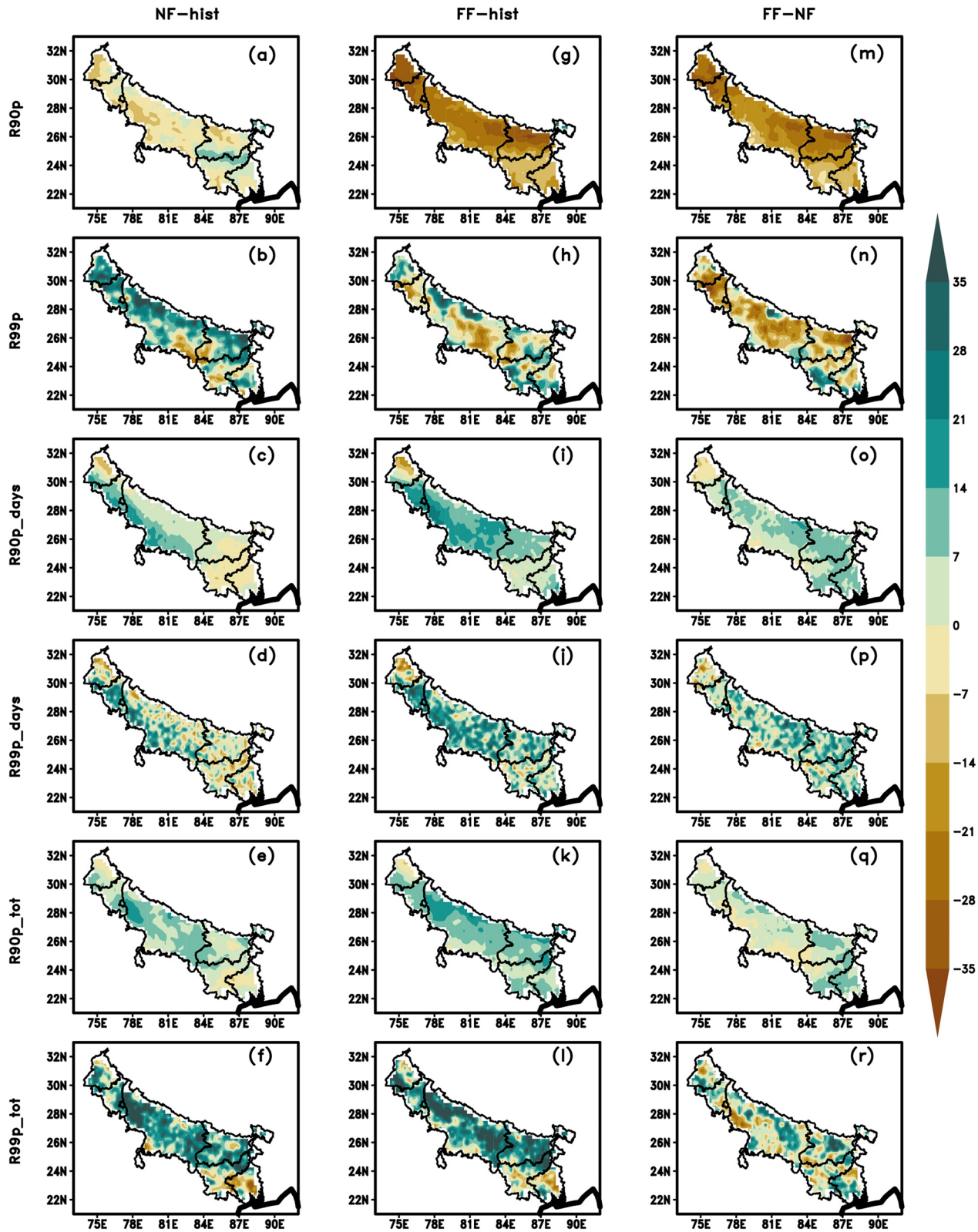

Figure 9. The spatial distribution of RegCM4 Projected relative changes (in %) under RCP8.5 scenario in various climate indices namely (a–c). R90p (d–f). R99p (g–i). R90p_days (j–l). R99p_days (m–o). R90p_tot (p–r). R99p_tot during near (NF-hist) and far future (FF-hist) as compared to the historical period and during far future as compared to the near future (FF-NF).

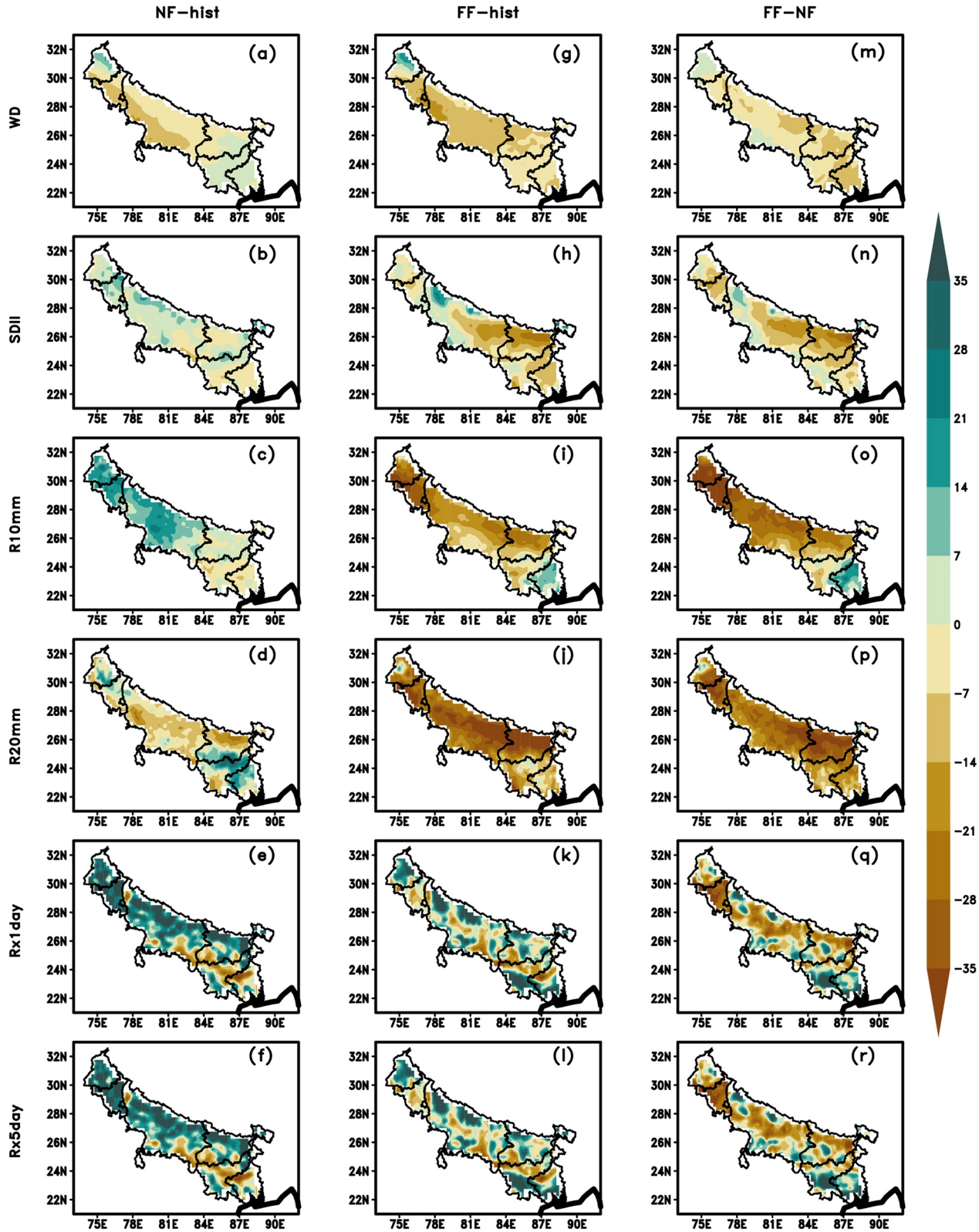

Figure 10. Same as Figure 9 but for climate indices namely (a–c). WD (d–f). SDII (g–i). R10 mm (j–l). R20 mm (m–o). Rx1day (p–r). Rx5day.

enhancement 7%–28% or more over almost entire IGP except extreme north-upper IGP where a small decrease nearly 7%–14% during FF have been projected (Figure 9n). Also, the projected changes over IGP region shows enhancement (7%–21%) during FF as compared to the NF with higher amount (∼14–21%) over lower IGP regions (Figure 9o). The RegCM4 projected pattern of R99p_tot depicts huge enhancement 21%–35% or more over most of the central IGP regions in NF (Figure 9p). Also, some south-upper IGP and north-lower IGP region shows moderate to high increase (14%–28%) in R99p_tot. Further, a decline 7%–28% over some isolated places of northern upper IGP and southern lower IGP have been projected in NF as compared with historical period. The FF projections of R99p_tot depicted similar pattern as that of during NF over entire IGP but with higher enhancement >35% over entire IGP region (Figure 9q). The projected changes during FF relative to the NF have shown moderate to high increase (7%–28%) over some north-central, south-upper and lower IGP regions (Figure 9r). However, a slight decline in R99p_tot (7%–21%) over south-central IGP regions have been projected during FF as compared with NF. The overall discussion suggests an increase in 90th and 99th percentiles of rainfall days and their contribution in ISMR over IGP under high emission RCP8.5 scenario. Some earlier researchers have proposed enhancement in extreme rainfall events over India and MCR during ISM season under warming future scenarios (Mukherjee et al., 2018; Pachauri et al., 2014; Sharmila et al., 2015) which also reflects in current study over IGP region.

In continuation to Figure 9, Figure 10 illustrates the relative changes in remaining climate indices during future time slices. The projected changes in WD suggest a slight to large decline (7%–14%) over central IGP while a slight increase over upper (14%) and lower IGP (7%) regions during NF as compared with the historical period (Figure 10a). Also, the RegCM4 FF projections show a moderate to higher decline (7%–21%) in WD over central IGP whereas higher increase (14%–21%) over some upper IGP regions (Figure 10b). However, the situation over the lower IGP region gets reversed during FF as compared with NF and a slight decline (7%) in WD can be noticed which also can be seen in the relative differences between FF-NF (Figure 10c). The decrease in WD resembles the study of Maharana et al. (2020) where they found a shift toward an arid climatic regime over almost the entire IGP region. Also, a study of Dash and Maity (2019) have found a decreasing trend in WD spells over the entire country during the recent decades. The distribution of mean or simple daily intensity that is, SDII shows moderate enhancement over most of the upper, central IGP regions during NF (Figure 10d). However, a moderate decline in SDII over most of the lower IGP regions has been projected. Further, the FF projections of SDII suggest 7%–21% of decrease over most of the lower and south-eastern central IGP regions (Figure 10e). A slight to higher increase (7%–28%) over some isolated regions in upper and north-central IGP can be noticed. A similar situation as that of FF-hist can also be noticed over entire IGP as far as the relative changes FF-NF are concerned (Figure 10f). The above analysis suggests that the number of WD and SDII may decrease over most of the IGP regions during JJAS in future under the high emission RCP8.5 scenario. Further, these results imply a decline in ISMR and possible shifts in monsoon and its features toward the later months of the year during the future under warming conditions (as discussed earlier in Section 3.5). The slight enhancement of WD and SDII over western IGP regions resembles the study of N. Singh and Sontakke (2002) where they proposed an increasing (decreasing) trend in ISMR over west (east) IGP regions.

The RegCM4 projected distribution pattern of changes in R10 mm days has been shown in Figures 10g–10i. Most of the IGP regions depicted enhancement (7%–28%) in the number of R10 mm days except a few southern-lower IGP regions where a very slight decrease of ∼7% in R10 mm days have been projected during NF as compared with historical period (Figure 10g). Surprisingly, the pattern of R10 mm gets reversed in RegCM4 FF projections as compared to the pattern during NF (Figure 10h). A moderate to higher decline (7%–35%) in number of R10 mm days over most of the IGP except few southern lower IGP regions where a slight increase of ∼ 7–21% have been projected during FF. The relative changes in FF as compared to NF also depicted a higher decline over most of the upper and central IGP while a rise over extremely lower IGP regions (Figure 10i). Similarly, the distribution of projected changes during NF in the number of R20 mm days shows a moderate to higher increase (7%–28%) over lower and some isolated upper IGP regions (Figure 10j). However, 7%–21% decrease over most of the central and extreme north-lower IGP has been projected during NF. Further, the FF projections of R20 mm suggest a 14%–35% or more decline in R20 mm days over almost entire IGP with massive changes being over northern regions of central and lower IGP (Figure 10k). However, a slight increase of ∼7% have been projected over some isolated places over lower and upper IGP during FF. The relative difference in the number of R20 mm days during FF-NF also depicted moderate to higher (14–28 or more) decline over entire IGP region (Figure 10l). The decline in WD, R10 mm and R20 mm may be a manifestation of enhanced atmospheric

aerosol over IGP and Indian ocean warming which causes a reduction in mean rainfall (Bollasina et al., 2011; V. Mishra et al., 2016). Also, evidence have been found in support of the weakening of monsoon circulation and delayed onsets over India (Shahi et al., 2021). The distribution of Rx1day shows very higher enhancement (21%–35% or more) over almost the entire IGP except for southern regions of central and lower IGP where moderate to higher (7%–28%) decline can be noticed in NF (Figure 10m). Further, the FF future projections suggest a scattered pattern with higher enhancement (21%–35% or more) over north-western, south-lower IGP and Himalayan foothill regions (Figure 10n). However, the rest of the regions have shown a moderate decline in Rx1day over IGP. The difference FF-NF depicts a moderate to higher decline in Rx1day over most of the upper and central IGP while massive enhancement over south-lower IGP regions (Figure 10o). The changes in Rx5day (Figure 10p-r) also a depict similar pattern as that of Rx1day over the entire IGP region during both the future time slices (NF & FF). The enhancement in extreme indices (RX1day and Rx5day) over foothills may be the manifestation of increased atmospheric aerosols under higher emission conditions (Choudhary et al., 2020; Lau et al., 2017).

4. Summary and Conclusions

This study accesses the characteristics of ISMR and associated extremes along with their possible future aspects over one of the most fluvial fertile lands across the globe. For that purpose, the second generation CORDEX-CORE simulations of RegCM4.7 have been considered. The RegCM4 with different forcings is able to produce the rainfall pattern satisfactorily along with its zonally distributed characteristics over the IGP region during the historical period. However, the statistical analysis suggests RegCM4 with forcings EIN75 and MPI-ESM-MR followed by MIROC5 and Nor-ESM performs robustly in simulating the rainfall patterns over the IGP. The RegCM4 has performed reasonably well in reproducing the patterns of various rainfall climate indices over IGP during the historical period. However, the overestimation of WD that is, the total number of wet days in RegCM4 simulations can be noticed which attributes to the inherent uncertainty in forcing data sets. Further, some extreme indices such as 90th and 99th percentiles of the distribution have shown maximum values near the Himalayan foothills which may be due to the increased aerosol accumulation over IGP.

The selection of RegCM4 member for the sake of future projections have been done by labeling a rank (1–4) based on the performance of an individual in simulating the area-averaged mean thresholds of indices during the historical period. The RegCM4 with the forcings MPI-ESM-MR and Nor-ESM have shown the least bias among all the members in simulating thresholds of different climate indices during the historical period. The future projections suggest slight variations in yearly mean rainfall while a huge decline in mean ISMR over IGP especially during FF. Also, the decline in the number of WD and SDII in the range of 7%–21% over the entire IGP except few western regions where increase ranging from ∼14% has been projected. The increasing WD and SDII over the western region may be an indication of changes from an arid to a humid regime. The contribution of 90th and 99th percentile that is, the upper tail or extreme rainfall days and their contribution in total ISMR may enhance by 7%–21% and 14%–35% respectively in future under high emission RCP8.5 scenario as can be seen in the projected patterns of R90p_days, R99p_days, R90p_tot and R99p_tot indices. The other extreme indices such as maximum 1-day and 5-day rainfall are also seeming to be intensified by 21%–35% over most of the IGP except lower IGP regions during the future under intense warming conditions. Focusing on the sub-regional scale, most of the extreme indices associated with 90th and 99th percentile of distribution show higher enhancement over upper and central IGP in future time slices. In addition to that massive increase in extremes has been projected over Himalayan foothills that is, the northern belt of almost the entire IGP region which may be a manifestation of enhanced anthropogenic aerosols under the RCP8.5 scenario. Contrary to that, over the lower IGP regions, a moderate to higher decline in extreme indices has been projected. Further, it has been found that the enhancement in these indices is less prominent during FF than in NF. These results indicate that there may be a weakening of monsoon circulations and a possible shift in monsoon season (other than JJAS months) over IGP in a warming climate. This study provides an overall assessment of ISMR characteristics and associated extremes over IGP in present as well as its possible future aspects under the high emission RCP8.5 scenario. The calculated thresholds of extreme indices may be used to define the regional criteria to define extreme rainfall events over IGP. The fertile land of IGP is the main source of food-grain and water supply for the huge Indian population, the outcomes of this study on IGP can be used as a reference to the policymakers to implement location-specific adaptation and mitigation measures.

Conflict of Interest

The authors declare no conflicts of interest relevant to this study.

Data Availability Statement

The gridded daily rainfall data (0.25° × 0.25°) is available at India Meteorological Department (IMD)'s 'Data Supply Portal' on payment basis (http://dsp.imdpune.gov.in/). The CORDEX-CORE simulation data sets are available freely in public domain at WCRP data portal (https://cordex.org/experiment-guidelines/cordex-core/). Further, the ERA5 reanalyses data sets can be accessed from the ECMWF data portal (https://www.ecmwf.int/en/forecasts/datasets/reanalysis-datasets/era5).

Acknowledgments
This work is a part of a DST funded R&D project. Authors wish to thank the WCRP community for initiating the CORDEX project, India Meteorology Department (IMD) for providing the data used in this study and ICTP for providing the RegCM4. One of the authors (RB) also acknowledges the IOE grant under Dev. Scheme 6031(A).

References

Alley, R. B., Marotzke, J., Nordhaus, W. D., Overpeck, J. T., Peteet, D. M., Pielke, R. A., Jr., et al. (2003). Abrupt climate change. *Science*, *299*(5615), 2005–2010. https://doi.org/10.1126/science.1081056

Ashfaq, M., Cavazos, T., Reboita, M. S., Torres-Alavez, J. A., Im, E.-S., Olusegun, C. F., et al. (2021). Robust late twenty-first century shift in the regional monsoons in RegCM-CORDEX simulations. *Climate Dynamics*, *57*(5), 1463–1488. https://doi.org/10.1007/s00382-020-05306-2

Ashfaq, M., Shi, Y., Tung, W. w., Trapp, R. J., Gao, X., Pal, J. S., & Diffenbaugh, N. S. (2009). Suppression of south Asian summer monsoon precipitation in the 21st century. *Geophysical Research Letters*, *36*(1), L01704. https://doi.org/10.1029/2008gl036500

Ayugi, B., Tan, G., Gnitou, G. T., Ojara, M., & Ongoma, V. (2020). Historical evaluations and simulations of precipitation over East Africa from Rossby Centre regional climate model. *Atmospheric Research*, *232*, 104705. https://doi.org/10.1016/j.atmosres.2019.104705

Baker, L. H., Collins, W. J., Olivié, D. J. L., Cherian, R., Hodnebrog, Ø., Myhre, G., & Quaas, J. (2015). Climate responses to anthropogenic emissions of short-lived climate pollutants. *Atmospheric Chemistry and Physics*, *15*(14), 8201–8216. https://doi.org/10.5194/acp-15-8201-2015

Bentsen, M., Bethke, I., Debernard, J. B., Iversen, T., Kirkevåg, A., Seland, Ø., et al. (2013). The Norwegian Earth system model, NorESM1-M–Part 1: Description and basic evaluation of the physical climate. *Geoscientific Model Development*, *6*(3), 687–720. https://doi.org/10.5194/gmd-6-687-2013

Bhatla, R., Ghosh, S., Mall, R., Sinha, P., & Sarkar, A. (2018). Regional climate model performance in simulating intra-seasonal and interannual variability of Indian summer monsoon. *Pure and Applied Geophysics*, *175*(10), 3697–3718. https://doi.org/10.1007/s00024-018-1886-x

Bhatla, R., Ghosh, S., Mandal, B., Mall, R., & Sharma, K. (2016). Simulation of Indian summer monsoon onset with different parameterization convection schemes of RegCM-4.3. *Atmospheric Research*, *176*, 10–18. https://doi.org/10.1016/j.atmosres.2016.02.010

Bhatla, R., Singh, M., Mall, R., Tripathi, A., & Raju, P. (2015). Variability of summer monsoon rainfall over Indo-Gangetic plains in relation to El-Nino/La-Nina. *Natural Hazards*, *78*(2), 837–853. https://doi.org/10.1007/s11069-015-1746-2

Bhatla, R., Varma, P., Verma, S., & Ghosh, S. (2020). El Nino/La Nina impact on crop production over different agro-climatic zones of Indo-Gangetic Plain of India. *Theoretical and Applied Climatology*, *142*, 151–163.

Bhatla, R., Verma, S., Pandey, R., & Tripathi, A. (2019). Evolution of extreme rainfall events over Indo-Gangetic plain in changing climate during 1901–2010. *Journal of Earth System Science*, *128*(5), 1–14. https://doi.org/10.1007/s12040-019-1162-1

Bollasina, M. A., Ming, Y., & Ramaswamy, V. (2011). Anthropogenic aerosols and the weakening of the South Asian summer monsoon. *Science*, *334*(6055), 502–505. https://doi.org/10.1126/science.1204994

Boyaj, A., Ashok, K., Ghosh, S., Devanand, A., & Dandu, G. (2018). The Chennai extreme rainfall event in 2015: The Bay of Bengal connection. *Climate Dynamics*, *50*(7), 2867–2879. https://doi.org/10.1007/s00382-017-3778-7

Canadell, J. G., Le Quéré, C., Raupach, M. R., Field, C. B., Buitenhuis, E. T., Ciais, P., et al. (2007). Contributions to accelerating atmospheric CO2 growth from economic activity, carbon intensity, and efficiency of natural sinks. *Proceedings of the National Academy of Sciences*, *104*(47), 18866–18870. https://doi.org/10.1073/pnas.0702737104

Chaturvedi, R. K., Joshi, J., Jayaraman, M., Bala, G., & Ravindranath, N. H. (2012). Multi-model climate change projections for India under representative concentration pathways. *Current Science*, 791–802.

Chaubey, P. K., Mall, R., Jaiswal, R., & Payra, S. (2022). Spatio-temporal changes in extreme rainfall events over different Indian River Basins. *Earth and Space Science*, *9*(3), e2021EA001930. https://doi.org/10.1029/2021ea001930

Chauhan, B. S., Mahajan, G., Randhawa, R. K., Singh, H., & Kang, M. S. (2014). Global warming and its possible impact on agriculture in India. *Advances in Agronomy*, *123*, 65–121.

Choudhury, G., Tyagi, B., Vissa, N. K., Singh, J., Sarangi, C., Tripathi, S. N., & Tesche, M. (2020). Aerosol-enhanced high precipitation events near the Himalayan foothills. *Atmospheric Chemistry and Physics*, *20*(23), 15389–15399. https://doi.org/10.5194/acp-20-15389-2020

Daloz, A. S., Rydsaa, J. H., Hodnebrog, Ø., Sillmann, J., van Oort, B., Mohr, C. W., et al. (2021). Direct and indirect impacts of climate change on wheat yield in the Indo-Gangetic plain in India. *Journal of Agriculture and Food Research*, *4*, 100132. https://doi.org/10.1016/j.jafr.2021.100132

Das, S., Giorgi, F., & Giuliani, G. (2020). Investigating the relative responses of regional monsoon dynamics to snow darkening and direct radiative effects of dust and carbonaceous aerosols over the Indian subcontinent. *Climate Dynamics*, *55*(3–4), 1011–1030. https://doi.org/10.1007/s00382-020-05307-1

Dash, S., & Maity, R. (2019). Temporal evolution of precipitation-based climate change indices across India: Contrast between pre-and post-1975 features. *Theoretical and Applied Climatology*, *138*(3), 1667–1678. https://doi.org/10.1007/s00704-019-02923-8

Donat, M., Alexander, L. V., Yang, H., Durre, I., Vose, R., Dunn, R. J., et al. (2013). Updated analyses of temperature and precipitation extreme indices since the beginning of the twentieth century: The HadEX2 dataset. *Journal of Geophysical Research: Atmospheres*, *118*(5), 2098–2118. https://doi.org/10.1002/jgrd.50150

Emanuel, K. A., & Živković-Rothman, M. (1999). Development and evaluation of a convection scheme for use in climate models. *Journal of the Atmospheric Sciences*, *56*(11), 1766–1782. https://doi.org/10.1175/1520-0469(1999)056<1766:daeoac>2.0.co;2

Fan, J., Rosenfeld, D., Zhang, Y., Giangrande, S. E., Li, Z., Machado, L. A., et al. (2018). Substantial convection and precipitation enhancements by ultrafine aerosol particles. *Science*, *359*(6374), 411–418. https://doi.org/10.1126/science.aan8461

Gadgil, S., & Gadgil, S. (2006). The Indian monsoon, GDP and agriculture. *Economic and Political Weekly*, 4887–4895.
Ghosh, S., Bhatla, R., Mall, R., Srivastava, P. K., & Sahai, A. (2019). Aspect of ECMWF downscaled Regional Climate Modeling in simulating Indian summer monsoon rainfall and dependencies on lateral boundary conditions. *Theoretical and Applied Climatology*, *135*(3), 1559–1581. https://doi.org/10.1007/s00704-018-2432-6
Ghosh, S., Sinha, P., Bhatla, R., Mall, R., & Sarkar, A. (2022). *Assessment of Lead-Lag and Spatial Errors in simulating different epochs of the Indian summer monsoon using RegCM4*, (p. 105892). Atmospheric Research.
Giorgi, F., & Bates, G. T. (1989). The climatological skill of a regional model over complex terrain. *Monthly Weather Review*, *117*(11), 2325–2347. https://doi.org/10.1175/1520-0493(1989)117<2325:tcsoar>2.0.co;2
Giorgi, F., Coppola, E., Solmon, F., Mariotti, L., Sylla, M., Bi, X., et al. (2012). RegCM4: Model description and preliminary tests over multiple CORDEX domains. *Climate Research*, *52*, 7–29. https://doi.org/10.3354/cr01018
Giorgi, F., Jones, C., & Asrar, G. R. (2009). Addressing climate information needs at the regional level: The CORDEX framework. *World Meteorological Organization Bulletin*, *58*(3), 175.
Goswami, B. N., Venugopal, V., Sengupta, D., Madhusoodanan, M., & Xavier, P. K. (2006). Increasing trend of extreme rain events over India in a warming environment. *Science*, *314*(5804), 1442–1445. https://doi.org/10.1126/science.1132027
Grenier, H., & Bretherton, C. S. (2001). A moist PBL parameterization for large-scale models and its application to subtropical cloud-topped marine boundary layers. *Monthly Weather Review*, *129*(3), 357–377. https://doi.org/10.1175/1520-0493(2001)129<0357:amppfl>2.0.co;2
Guhathakurta, P., Menon, P., Inkane, P., Krishnan, U., & Sable, S. (2017). Trends and variability of meteorological drought over the districts of India using standardized precipitation index. *Journal of Earth System Science*, *126*(8), 1–18. https://doi.org/10.1007/s12040-017-0896-x
Herold, N., Behrangi, A., & Alexander, L. V. (2017). Large uncertainties in observed daily precipitation extremes over land. *Journal of Geophysical Research: Atmospheres*, *122*(2), 668–681. https://doi.org/10.1002/2016jd025842
Hoffman, R. N., Boukabara, S.-A., Kumar, V. K., Garrett, K., Casey, S. P., & Atlas, R. (2017). An empirical cumulative density function approach to defining summary NWP forecast assessment metrics. *Monthly Weather Review*, *145*(4), 1427–1435. https://doi.org/10.1175/mwr-d-16-0271.1
Kang, I.-S., Yang, Y.-M., & Tao, W.-K. (2015). GCMs with implicit and explicit representation of cloud microphysics for simulation of extreme precipitation frequency. *Climate Dynamics*, *45*(1–2), 325–335. https://doi.org/10.1007/s00382-014-2376-1
Kiehl, J., Hack, J., Bonan, G., Boville, B., Briegleb, B., Williamson, D., & Rasch, P. (1996). *Description of the NCAR community climate model (CCM3)*. NCAR Technical Note.
Kitoh, A., & Endo, H. (2016). Changes in precipitation extremes projected by a 20-km mesh global atmospheric model. *Weather and Climate Extremes*, *11*, 41–52. https://doi.org/10.1016/j.wace.2015.09.001
Kothyari, U., Singh, V., & Aravamuthan, V. (1997). An investigation of changes in rainfall and temperature regimes of the Ganga Basin in India. *Water Resources Management*, *11*(1), 17–34. https://doi.org/10.1023/a:1017936123283
Kumar, K. K., Patwardhan, S., Kulkarni, A., Kamala, K., Rao, K. K., & Jones, R. (2011). Simulated projections for summer monsoon climate over India by a high-resolution regional climate model (PRECIS). *Current Science*, 312–326.
Lau, W. K., Kim, K. M., Shi, J. J., Matsui, T., Chin, M., Tan, Q., et al. (2017). Impacts of aerosol–monsoon interaction on rainfall and circulation over Northern India and the Himalaya Foothills. *Climate Dynamics*, *49*(5–6), 1945–1960. https://doi.org/10.1007/s00382-016-3430-y
Luwangleima, M., & Shrivastava, S. K. (2019). Variations of daily extreme precipitation over stations of humid north-east India. *Indian Journal of Hill Farming*, *32*(1), 131–136.
Maharana, P., & Dimri, A. (2016). Study of intraseasonal variability of Indian summer monsoon using a regional climate model. *Climate Dynamics*, *46*(3–4), 1043–1064. https://doi.org/10.1007/s00382-015-2631-0
Maharana, P., Dimri, A., & Choudhary, A. (2020). Future changes in Indian summer monsoon characteristics under 1.5 and 2° C specific warming levels. *Climate Dynamics*, *54*(1), 507–523. https://doi.org/10.1007/s00382-019-05012-8
Maity, R., Aggarwal, A., & Chanda, K. (2016). Do CMIP5 models hint at a warmer and wetter India in the 21st century? *Journal of Water and Climate Change*, *7*(2), 280–295. https://doi.org/10.2166/wcc.2015.126
Maity, S., Satyanarayana, A. N. V., Mandal, M., & Nayak, S. (2017). Performance evaluation of land surface models and cumulus convection schemes in the simulation of Indian summer monsoon using a regional climate model. *Atmospheric Research*, *197*, 21–41. https://doi.org/10.1016/j.atmosres.2017.06.023
Mishra, A. K., Dwivedi, S., & Das, S. (2020). Role of Arabian Sea warming on the Indian summer monsoon rainfall in a regional climate model. *International Journal of Climatology*, *40*(4), 2226–2238. https://doi.org/10.1002/joc.6328
Mishra, V., Aadhar, S., Asoka, A., Pai, S., & Kumar, R. (2016). On the frequency of the 2015 monsoon season drought in the Indo-Gangetic Plain. *Geophysical Research Letters*, *43*(23), 12102–112112. https://doi.org/10.1002/2016gl071407
Mishra, V., & Shah, H. L. (2018). Hydroclimatological perspective of the Kerala flood of 2018. *Journal of the Geological Society of India*, *92*(5), 645–650. https://doi.org/10.1007/s12594-018-1079-3
Mukherjee, S., Aadhar, S., Stone, D., & Mishra, V. (2018). Increase in extreme precipitation events under anthropogenic warming in India. *Weather and Climate Extremes*, *20*, 45–53. https://doi.org/10.1016/j.wace.2018.03.005
Ngo-Duc, T., Tangang, F. T., Santisirisomboon, J., Cruz, F., Trinh-Tuan, L., Nguyen-Xuan, T., et al. (2017). Performance evaluation of RegCM4 in simulating extreme rainfall and temperature indices over the CORDEX-Southeast Asia region. *International Journal of Climatology*, *37*(3), 1634–1647. https://doi.org/10.1002/joc.4803
O'Gorman, P. A., & Schneider, T. (2009). The physical basis for increases in precipitation extremes in simulations of 21st-century climate change. *Proceedings of the National Academy of Sciences*, *106*(35), 14773–14777. https://doi.org/10.1073/pnas.0907610106
Oleson, K., Lawrence, D., Bonan, G., Drewniak, B., Huang, M., Koven, C., et al. (2013). *Technical description of version 4.5 of the community land model (CLM) (No. NCAR/TN-503+ STR)*. UCAR.
Pachauri, R. K., Allen, M. R., Barros, V. R., Broome, J., Cramer, W., Christ, R., et al. (2014). Climate change 2014: Synthesis report. *Contribution of Working Groups I, II and III to the fifth assessment report of the Intergovernmental Panel on Climate Change*. IPCC.
Pai, D., Rajeevan, M., Sreejith, O., Mukhopadhyay, B., & Satbha, N. (2014). Development of a new high spatial resolution (0.25× 0.25) long period (1901-2010) daily gridded rainfall data set over India and its comparison with existing data sets over the region. *Mausam*, *65*(1), 1–18. https://doi.org/10.54302/mausam.v65i1.851
Pal, D., Bhattacharyya, T., Srivastava, P., Chandran, P., & Ray, S. (2009). Soils of the Indo-Gangetic plains: Their historical perspective and management. *Current Science*, 1193–1202.
Pal, J. S., Giorgi, F., Bi, X., Elguindi, N., Solmon, F., Gao, X., et al. (2007). Regional climate modeling for the developing world: The ICTP RegCM3 and RegCNET. *Bulletin of the American Meteorological Society*, *88*(9), 1395–1410. https://doi.org/10.1175/bams-88-9-1395
Pal, J. S., Small, E. E., & Eltahir, E. A. (2000). Simulation of regional-scale water and energy budgets: Representation of subgrid cloud and precipitation processes within RegCM. *Journal of Geophysical Research*, *105*(D24), 29579–29594. https://doi.org/10.1029/2000jd900415

Panda, D. K., Panigrahi, P., Mohanty, S., Mohanty, R. K., & Sethi, R. R. (2016). The 20th century transitions in basic and extreme monsoon rainfall indices in India: Comparison of the ETCCDI indices. *Atmospheric Research*, *181*, 220–235. https://doi.org/10.1016/j.atmosres.2016.07.002

Pant, M., Ghosh, S., Verma, S., Sinha, P., Mall, R. K., & Bhatla, R. (2022). Simulation of an extreme rainfall event over Mumbai using a regional climate model: A case study. *Meteorology and Atmospheric Physics*, *134*(1), 1–17. https://doi.org/10.1007/s00703-021-00845-7

Pattanaik, D. R., & Rajeevan, M. (2010). Variability of extreme rainfall events over India during southwest monsoon season. *Meteorological Applications: A journal of forecasting, practical applications, training techniques and modelling*, *17*(1), 88–104. https://doi.org/10.1002/met.164

Rai, P., Singh, G., & Dash, S. (2020). Projected changes in extreme precipitation events over various subdivisions of India using RegCM4. *Climate Dynamics*, *54*(1), 247–272. https://doi.org/10.1007/s00382-019-04997-6

Rajeevan, M., Gadgil, S., & Bhate, J. (2010). Active and break spells of the Indian summer monsoon. *Journal of Earth System Science*, *119*(3), 229–247. https://doi.org/10.1007/s12040-010-0019-4

Reshma, T., Varikoden, H., & Babu, C. A. (2021). Observed changes in Indian summer monsoon rainfall at different intensity bins during the past 118 years over five homogeneous regions. *Pure and Applied Geophysics*, *178*(9), 3655–3672. https://doi.org/10.1007/s00024-021-02826-8

Rosenfeld, D., Woodley, W. L., Khain, A., Cotton, W. R., Carrió, G., Ginis, I., & Golden, J. H. (2012). Aerosol effects on microstructure and intensity of tropical cyclones. *Bulletin of the American Meteorological Society*, *93*(7), 987–1001. https://doi.org/10.1175/bams-d-11-00147.1

Roxy, M. K., Ghosh, S., Pathak, A., Athulya, R., Mujumdar, M., Murtugudde, R., et al. (2017). A threefold rise in widespread extreme rain events over central India. *Nature Communications*, *8*(1), 1–11. https://doi.org/10.1038/s41467-017-00744-9

Roxy, M. K., Ritika, K., Terray, P., & Masson, S. (2014). The curious case of Indian Ocean warming. *Journal of Climate*, *27*(22), 8501–8509. https://doi.org/10.1175/jcli-d-14-00471.1

Roxy, M. K., Ritika, K., Terray, P., Murtugudde, R., Ashok, K., & Goswami, B. (2015). Drying of Indian subcontinent by rapid Indian Ocean warming and a weakening land-sea thermal gradient. *Nature Communications*, *6*(1), 1–10. https://doi.org/10.1038/ncomms8423

Roy, S. S., & Balling, R. C. (2004). Trends in extreme daily precipitation indices in India. *International Journal of Climatology*, *24*(4), 457–466. https://doi.org/10.1002/joc.995

Samuel, S., Wiston, M., Mphale, K., & Faka, D. N. (2021). Changes in extreme precipitation events in the Zambezi River basins based on CORDEX-CORE models, Part II: Future projections under 1.5, 2.0, and 3.0°C global warming levels. *International Journal of Climatology*, *42*(11), 5467–5486. https://doi.org/10.1002/joc.7543

Sanjay, J., Krishnan, R., Shrestha, A. B., Rajbhandari, R., & Ren, G.-Y. (2017). Downscaled climate change projections for the Hindu Kush Himalayan region using CORDEX South Asia regional climate models. *Advances in Climate Change Research*, *8*(3), 185–198. https://doi.org/10.1016/j.accre.2017.08.003

Shahi, N. K. (2022). Fidelity of the latest high-resolution CORDEX-CORE regional climate model simulations in the representation of the Indian summer monsoon precipitation characteristics. *Climate Dynamics*, 1–23. https://doi.org/10.1007/s00382-022-06602-9

Shahi, N. K., Das, S., Ghosh, S., Maharana, P., & Rai, S. (2021). Projected changes in the mean and intra-seasonal variability of the Indian summer monsoon in the RegCM CORDEX-CORE simulations under higher warming conditions. *Climate Dynamics*, *57*(5–6), 1–18. https://doi.org/10.1007/s00382-021-05771-3

Sharmila, S., Joseph, S., Sahai, A., Abhilash, S., & Chattopadhyay, R. (2015). Future projection of Indian summer monsoon variability under climate change scenario: An assessment from CMIP5 climate models. *Global and Planetary Change*, *124*, 62–78. https://doi.org/10.1016/j.gloplacha.2014.11.004

Sillmann, J., Kharin, V. V., Zwiers, F. W., Zhang, X., & Bronaugh, D. (2013). Climate extremes indices in the CMIP5 multimodel ensemble: Part 2. Future climate projections. *Journal of Geophysical Research: Atmospheres*, *118*(6), 2473–2493. https://doi.org/10.1002/jgrd.50188

Simpkins, G. (2017). Hydroclimate: Extreme rain in India. *Nature Climate Change*, *7*(11), 760. https://doi.org/10.1038/nclimate3429

Singh, D., Tsiang, M., Rajaratnam, B., & Diffenbaugh, N. S. (2014). Observed changes in extreme wet and dry spells during the South Asian summer monsoon season. *Nature Climate Change*, *4*(6), 456–461. https://doi.org/10.1038/nclimate2208

Singh, N., & Sontakke, N. (2002). On climatic fluctuations and environmental changes of the Indo-Gangetic plains, India. *Climatic Change*, *52*(3), 287–313. https://doi.org/10.1023/a:1013772505484

Singh, S., Ghosh, S., Sahana, A., Vittal, H., & Karmakar, S. (2017). Do dynamic regional models add value to the global model projections of Indian monsoon? *Climate Dynamics*, *48*(3), 1375–1397. https://doi.org/10.1007/s00382-016-3147-y

Sinha, P., Maurya, R., Mohanty, M., & Mohanty, U. (2019). Inter-comparison and evaluation of mixed-convection schemes in RegCM4 for Indian summer monsoon simulation. *Atmospheric Research*, *215*, 239–252. https://doi.org/10.1016/j.atmosres.2018.09.002

Solomon, S., Manning, M., Marquis, M., & Qin, D. (2007). Climate change 2007-the physical science basis. In *Working group I contribution to the fourth assessment report of the IPCC* (Vol. 4). Cambridge university press.

Sonkoué, D., Monkam, D., Fotso-Nguemo, T. C., Yepdo, Z. D., & Vondou, D. A. (2019). Evaluation and projected changes in daily rainfall characteristics over Central Africa based on a multi-model ensemble mean of CMIP5 simulations. *Theoretical and Applied Climatology*, *137*(3), 2167–2186. https://doi.org/10.1007/s00704-018-2729-5

Stevens, B., Giorgetta, M., Esch, M., Mauritsen, T., Crueger, T., Rast, S., et al. (2013). Atmospheric component of the MPI-M Earth system model: ECHAM6. *Journal of Advances in Modeling Earth Systems*, *5*(2), 146–172. https://doi.org/10.1002/jame.20015

Tabari, H. (2020). Climate change impact on flood and extreme precipitation increases with water availability. *Scientific Reports*, *10*(1), 1–10. https://doi.org/10.1038/s41598-020-70816-2

Tao, W. K., Chen, J. P., Li, Z., Wang, C., & Zhang, C. (2012). Impact of aerosols on convective clouds and precipitation. *Reviews of Geophysics*, *50*(2). https://doi.org/10.1029/2011rg000369

Taylor, K. E. (2001). Summarizing multiple aspects of model performance in a single diagram. Journal of Geophysical Research. *Atmosphere*, *106*(D7), 7183–7192. https://doi.org/10.1029/2000jd900719

Tegegne, G., Melesse, A. M., & Alamirew, T. (2021). Projected changes in extreme precipitation indices from CORDEX simulations over Ethiopia, East Africa. *Atmospheric Research*, *247*, 105156. https://doi.org/10.1016/j.atmosres.2020.105156

Tiedtke, M. (1989). A comprehensive mass flux scheme for cumulus parameterization in large-scale models. *Monthly Weather Review*, *117*(8), 1779–1800. https://doi.org/10.1175/1520-0493(1989)117<1779:acmfsf>2.0.co;2

Tollefson, J. (2020). How hot will Earth get by 2100? *Nature*, *580*(7804), 443–446. https://doi.org/10.1038/d41586-020-01125-x

Turner, A. G., & Annamalai, H. (2012). Climate change and the South Asian summer monsoon. *Nature Climate Change*, 2(8), 587–595. https://doi.org/10.1038/nclimate1495

Verma, S., & Bhatla, R. (2021). Performance of RegCM4 for dynamically downscaling of El Nino/La Nina events during southwest monsoon over India and its regions. *Earth and Space Science*, *8*(3), e2020EA001474. https://doi.org/10.1029/2020ea001474

Verma, S., Bhatla, R., Ghosh, S., Sinha, P., Kumar Mall, R., & Pant, M. (2021). Spatio-temporal variability of summer monsoon surface air temperature over India and its regions using Regional Climate Model. *International Journal of Climatology*, *41*(13), 5820–5842. https://doi.org/10.1002/joc.7155

Verma, S., Bhatla, R., Shahi, N., & Mall, R. (2022). Regional modulating behavior of Indian summer monsoon rainfall in context of spatio-temporal variation of drought and flood events. *Atmospheric Research*, *274*, 106201. https://doi.org/10.1016/j.atmosres.2022.106201

Vinnarasi, R., & Dhanya, C. (2016). Changing characteristics of extreme wet and dry spells of Indian monsoon rainfall. *Journal of Geophysical Research: Atmospheres*, *121*(5), 2146–2160. https://doi.org/10.1002/2015jd024310

Watanabe, S., & Opper, M. (2010). Asymptotic equivalence of Bayes cross validation and widely applicable information criterion in singular learning theory. *Journal of Machine Learning Research*, *11*(12).

Wu, Y., Xu, X.-J., & Gao, X. J. (2017). Projected changes in mean and extreme climates over Hindu Kush Himalayan region by 21 CMIP5 models. *Advances in Climate Change Research*, *8*(3), 176–184. https://doi.org/10.1016/j.accre.2017.03.001

Yaduvanshi, A., Nkemelang, T., Bendapudi, R., & New, M. (2021). Temperature and rainfall extremes change under current and future global warming levels across Indian climate zones. *Weather and Climate Extremes*, *31*, 100291. https://doi.org/10.1016/j.wace.2020.100291

Yaduvanshi, A., & Ranade, A. (2017). Long-term rainfall variability in the Eastern Gangetic plain in relation to global temperature change. *Atmosphere-Ocean*, *55*(2), 94–109. https://doi.org/10.1080/07055900.2017.1284041

Zhang, X., Alexander, L., Hegerl, G. C., Jones, P., Tank, A. K., Peterson, T. C., et al. (2011). Indices for monitoring changes in extremes based on daily temperature and precipitation data. *Wiley Interdisciplinary Reviews: Climate Change*, *2*(6), 851–870. https://doi.org/10.1002/wcc.147